Ab initio metadynamics determination of temperature-dependent free-energy landscape in ultrasmall silver clusters

by

Daniel Sucerquia Gaviria

A dissertation submitted in partial fulfillment
of the requirements for the degree of

Master of Physics

Advisor: Olga Lucía López, Ph.D.
Co-advisor: Pilar Cossio, Ph.D.

Faculty of Exact and Natural Sciences
May, 2022

Acknowledgments

My most sincere thanks to my advisor, Olga Lopez, and my co-advisor, Pilar Cossio, for their trust, patience, understanding, and effort to help me succeed. I am very grateful for their advice and criticism throughout this pivotal point in my professional and personal growth. I am very happy to have had them as my advisors. Among many more reasons, I thank them for their help to find opportunities for my future. My special gratitude to Olga, for our constant discussions about computation, teaching, and learning techniques.

I am also grateful for the members of the Max Planck Tandem group for their help and discussions.

I want to thank my family for showing their pride in me and for their support in difficult times, even though my academic commitments meant my absence in a few important moments.

Finally, my gratitude to the University of Antioquia for the “Student Instructor” program that granted the funding, gave me the opportunity to complete this degree, and allowed me to have my first experience as an instructor at the university level. I would also like to thank the Max Planck Tandem group for their financial support.

To my family, especially my nephew and niece

Abstract

This thesis concerns the study of the influence of temperature and environmental effects in silver clusters at different temperatures. In particular, we reconstruct the free energy surface of Ag_2, Ag_5 and Ag_6.

For Ag_5 and Ag_6, we apply *ab-initio* Well-Tempered Metadynamics simulations at different temperatures. This is based on the Born-Oppenheimer Approximation and Density Functional Theory (DFT) to describe inter-atomic forces of the electronic distribution. Then, we evolve the system by adding an artificial bias potential to explore different regions of the configuration landscape and to estimate the free energy surface at 10, 100, and 300 K with the radius of gyration and coordination number as collective variables, finding errors, at most, in the order of tens of meV. Relative free-energy differences between the planar and non-planar isomers of both clusters decrease with temperature, in agreement with the previously proposed stabilization of non-planar isomers. Interestingly, we find that Ag_6 is the smallest silver cluster where entropic effects at room temperature boost the non planar isomer probability to a significant value, making probable a mixture of isomers. This way, we obtain thermal effects over the probability of each state of the system.

For Ag_2, we reconstruct the free energy surface of the dissociation process of a silver dimer, considering a water solvent environment. Here, we use the ASE-PLUMED interface to apply Quantum Mechanics/Molecular Mechanics (QM/MM) with Well-Tempered Metadynamics, where the silver dimer is described with quantum mechanics and the water molecules are classical. We use the distance between the silver atoms as the collective variable. We show that the addition of water molecules in the simulation promotes the dissociation process, decreasing the free-energy barrier between the bounded and unbounded states. Unlike the vacuum model, in the solvent embedded case, we find that forming a dimer bond requires a barrier-crossing.

To perform these simulations, we develop an interface between the atomic simulation environment (ASE) and the PLUMED plug-in. This interface enables performing enhanced sampling techniques and molecular dynamics analysis using quantum and classical codes implemented in ASE. We show the details of this development and present the tests to prove the correct performance of the interface. This new ASE-PLUMED interface enables simulating

nanosystem electronic properties at more realistic conditions. These methods can help better describe larger nanoclusters and can be improved considering interactions with other environments.

Contents

List of figures

List of Tables

List of Abbreviations

BOA	Born Oppenheimer Approximation
DFT	Density Functional Theory
CV	Collective variable
MTD	Metadynamics
PAW	Projected Augmented Wave
QM/MM	Quantum Mechanics/Molecular Mechanics
WT-MTD	Well-Tempered Metadynamics

All things are made of atoms - little particles that move around in perpetual motion, attracting each other when they are a little distance apart, but repelling upon being squeezed into one another. In that one sentence, you will see, there is an enormous amount of information about the world, if just a little imagination and thinking are applied.

Richard P. Feynman

1 Introduction

Noble metal nanoclusters have attracted much attention due to their molecular-like properties and high luminescence with potential applications in catalysis, biosensing, and bioimaging[1]. Silver nanoclusters, both bare and ligand-stabilized, have a particular ability to form diverse structural motifs and a rich variety of isomers[2]. The experimental and simulated absorption spectrum of ultrasmall bare silver clusters indicates the coexistence of several isomers even at low temperatures starting at N=6 – with N the number of atoms in the cluster –, and a transition from a planar structure to a three-dimensional structure for its lower energy isomer at N=7[3,4,5]. This transition to non-planar structures is therefore much faster than its gold equivalent, which is placed at N=11 up to temperature T=100K[6,7].

We can study these clusters computationally using Metadynamics (MTD) that is a free-energy estimation method that allows to explore the conformational space of a system at a given temperature. It relies on the theoretical relation between the free energy of the system and a bias potential that drives the system to cross barriers and explore new conformations[8,9]. In principle, such algorithms can be coupled to any energy-force level description of the system. However, most applications prefer classical to quantum methods. Metadynamics with quantum methods has been used to simulate chemical and biochemical reactions in the gas phase, solid phase, and in solution using Car Parrinello[10], Born-Oppenheimer molecular dynamics[11], and QM/MM metadynamics[12]. Some applications, for example, are allyl cyanide to pirrole isomerization[13], formation of silver-chloro complexes[14], and water splitting and H_2 evolution by Ru(II)-Pincer complexes[15]. To overcome the limitation of short trajectories

which are typical of quantum methods, minimum activation barriers have been reported to stop the metadynamics trajectory once the first transition is achieved. They have also been reported to average over a few resulting barriers[15,16] or to continue a single trajectory, stopping the dynamics after one recrossing has been achieved[17,18]. The lack of a good estimation of the resulting errors out of such short trajectories is hindering a more extended use of this important free-energy estimation method.

How could the isomerization of silver clusters depend on temperature? Could the 2D-3D transition depend on temperature and other experimental conditions? Such questions require an estimation of the free-energy landscape of small silver clusters. A few studies on gold clusters have started to address these questions with the combination of quantum methods and enhanced sampling methods. Metadynamics applied to Au_{12} clusters[19] shows that, at room temperature, there is an equiprobable mixture of isomers. Recent work[7] on gold clusters predicts that, at T=300K with N=8 atoms, there are non-planar isomers with non-negligible probabilities competing with planar isomers.

Our goal is to accurately determine the temperature-dependent free-energy landscape of small neutral clusters with the use of *ab-initio* metadynamics in a general purpose interface. We also propose to include the effect of the environment in the free-energy landscape of Ag_2 dissociation, using Quantum Mechanics/Molecular Mechanics (QM/MM). These results are useful to address questions of isomerization and the influence of solvents or organic matter stabilizing certain isomers. Accurate free-energy landscapes can also be used as a benchmark for classical force field developments[20].

In the following section, we present the problem statement, hypothesis and objectives of this work. In Chapter 2, we present the theory that supports our work, including Density Functional Theory, principles of statistical mechanics, and details on enhanced sampling methods. Chapter 3 introduces the computational methods implemented in the codes we used: the atomic simulation environment (ASE), the grid projected augmented wave (GPAW) and the plug-in PLUMED. It also contains a detailed explanation of the developed interface between ASE and PLUMED and its validation tests. Chapter 4 presents the implementation of the interface and a detailed discussion, including parameter selection and error determination. Finally, we close this work with our conclusions and perspectives. Furthermore, three appendixes contain additional information: the academic products of this thesis, the calculator we created, the tests included in the official version of ASE, and specific examples of silver configurations.

1.1 Problem Statement

Since the proposal of the electronic shell model[21], theoretical and computational modeling have played a pivotal role in the exploration of bare and protected noble metal clusters. One of the open questions in the literature that computation can help answer is: what are the conformations of silver clusters in realistic environments? The typical way to deal with this problem is to study the structure that minimizes the ground-state potential energy. However, this zero-temperature approximation neglects the possible influence of thermal aspects, which could play an important role in the description of the system of interest. Thus, it is necessary to consider entropic effects to obtain a complete exploration of accessible conformations and their corresponding probability.

However, it is not easy to achieve a complete exploration of the conformational landscape of molecular systems or to extract the probability distribution and the lifetimes of states. Molecular Dynamics (MD) propose to tackle this problem by simulating the time evolution of the system, assuming a complete exploration of the relevant states driven by thermal fluctuations. However, high free-energy barriers –with respect to the thermal energy (k_BT)– are an obstacle for MD simulations, as obtaining transitions between states is not guaranteed, even after long simulated times. This problem is even greater for simulations that consider quantum approximations, due to the computational effort needed for this kind of calculations.

As an alternative, enhanced sampling methods, such as Metadynamics, accelerate the exploration of the configuration landscape by adding a biasing potential to push the system towards different configurations and estimate the free-energy surface from said added bias. Even so, there is no standard criterion of convergence to accurately estimate the free-energy surface. This is a possible reason as to why enhanced sampling methods are widely implemented in biophysics but scarcely applied to nanomaterials. Indeed, codes that combined enhanced sampling with QM accuracy calculations were rare and not widely available.

1.2 Hypothesis

Environmental and thermal aspects affect the stability of the states of ultra-small silver clusters. These effects can be described in ASE using *ab-initio* Well-Tempered Metadynamics simulations with a set of collective variables that guarantee a convergence to the free-energy surface.

1.3 Objectives

General Objective

To estimate the free energy of different silver clusters with an interface between ASE and PLUMED using *ab-initio* Well-Tempered Metadynamics.

Specific Objectives

- Develop and test a code in the official version of ASE interfaced with PLUMED.
- Explore different collective variables and parameters of the simulations of silver clusters to optimize the estimation of the free-energy surface.
- Extract the free-energy surface of Ag_5 and Ag_6 in gas phase at 10, 100, and 300 K using *ab-initio* Well Tempered Metadynamics in ASE, while maintaining the error in the order of tens of meV.
- Study the dissociation process of a silver dimer at 300K, including liquid water solvent effects, with QM/MM.

2 Theory

2.1 Summary

For our study, we assume the Born-Oppenheimer Approximation for separating the electronic and nuclear dynamics. The electronic component is solved using Zero-temperature Density Functional Theory (DFT)[22], which finds the density associated with the ground-state electronic solution. The electronic density enables the computation of the interatomic forces. We can add classical atoms to this formalism to, for example, include solvent effects. With the computed forces, we can simulate a time evolution of the system to sample different conformations. Moreover, using Metadynamics and a set of collective variables, we can accelerate the exploration of specific degrees of freedom in order to push the systems towards different configurations. These simulations generate a reconstruction of the free-energy surface, which is directly related to the probability of the configurations and, therefore, with the statistical properties of each state.

In this chapter, we detail the theory behind the methods used in this thesis.

2.2 Density Functional Theory

In this section, we present how to obtain interatomic forces by applying quantum approximations in the solution of the electronic distribution. We use these forces for solving the classical equations of motion of the atoms.

2.2.1 Electronic and Nuclear Dynamic Separation with the Born-Oppenheimer Approximation

The Hamiltonian that represents the complete system of nucleus and electrons can be written as[22]

$$\hat{H}_{tot} = \hat{T}_n + \hat{T}_e + \hat{V}_{ne} + \hat{V}_{ee} + \hat{V}_{nn} \,, \tag{2.1}$$

where $\hat{T}_n$ and $\hat{T}_e$ are the operators associated with the kinetic energy of the nucleus and the electrons, respectively; and $\hat{V}_{ne}$, $\hat{V}_{ee}$ and $\hat{V}_{nn}$ are the potential energy operators that contain the nucleus-electron, electron-electron, and nucleus-nucleus interactions, in that order. We can re-write this Hamiltonian in terms of the electronic Hamiltonian (H_e),

$$\hat{H}_{tot} = \hat{T}_n + \hat{H}_e \,, \tag{2.2}$$

$$\hat{H}_e = \hat{T}_e + \hat{V}_{ne} + \hat{V}_{ee} + \hat{V}_{nn} \,. \tag{2.3}$$

Note that H_e depends on the positions of the nucleus. Because of the expected different electron and nucleus time scales, one can assume and search for solutions to H_e where the nucleus contribution is parametric. As the electronic Hamiltonian is Hermitic, there must exist a set of orthonormal eigenfunctions Φ of this operator, in terms of the N_e electronic coordinates $\mathbf{r} = (\mathbf{r}_1, ..., \mathbf{r}_{N_e})$ and parametrized by the coordinates of the N nucleus, $\mathbf{R} = (\mathbf{R}_1, ..., \mathbf{R}_N)$, so that

$$\hat{H}_e(\mathbf{R})\Phi_i(\mathbf{r};\mathbf{R}) = \varepsilon_i(\mathbf{R})\Phi_i(\mathbf{r};\mathbf{R}) \,, \tag{2.4}$$

$$\int \Phi_i^*(\mathbf{r};\mathbf{R})\Phi_j(\mathbf{r};\mathbf{R})d\mathbf{r} = \delta_{ij} \,. \tag{2.5}$$

This basis set can be used to expand the total wave function of the system, considering the coefficients as functions χ of the nucleus coordinates $\mathbf{R}$,

$$\Psi_k(\mathbf{R},\mathbf{r}) = \sum_{i=1}^{\infty} \chi_{ik}(\mathbf{R})\Phi_i(\mathbf{r};\mathbf{R}) \,. \tag{2.6}$$

So, the time-independent Schrödinger equation in this basis can be written as

$$\hat{H}_{tot}\Psi_k = E_k\Psi_k \tag{2.7}$$

$$\Rightarrow \left(\hat{T}_n + \hat{H}_e\right)\left(\sum_{i=1}^{\infty}\chi_{ik}\Phi_i\right) = E_k\left(\sum_{i=1}^{\infty}\chi_{ik}\Phi_i\right) \tag{2.8}$$

$$\Rightarrow \sum_{i=1}^{\infty}\left(\hat{T}_n\chi_{ik}\Phi_i + \chi_{ik}\hat{H}_e\Phi_i\right) = E_k\left(\sum_{i=1}^{\infty}\chi_{ik}\Phi_i\right) , \tag{2.9}$$

where, for the sake of simplicity, we use $\Psi_k = \Psi_k(\mathbf{R},\mathbf{r})$, $\chi_{ik} = \chi_{ik}(\mathbf{R})$ and $\Phi_i = \Phi_i(\mathbf{r};\mathbf{R})$. We define $\nabla_R^2 = \hat{T}_n = -\sum_a \frac{1}{2M_a}\nabla_a^2$ where a is the index of the nucleus (also named ion). Taking advantage of the linearity of the operator ∇_a^2, which only affects the nuclei coordinates, $\mathbf{R}$, it yields

$$\sum_{i=1}^{\infty}\left(\nabla_R^2(\chi_{ik}\Phi_i) + \chi_{ik}\hat{H}_e\Phi_i\right) = E_k\left(\sum_{i=1}^{\infty}\chi_{ik}\Phi_i\right) \tag{2.10}$$

$$\Rightarrow \sum_{i=1}^{\infty}\begin{pmatrix}\Phi_i{\nabla_R}^2\chi_{ik} + 2\nabla_R\chi_{ik}\cdot\nabla_R\Phi_i + \\ \chi_{ik}{\nabla_R}^2\Phi_i + \varepsilon_i\chi_{ik}\Phi_i\end{pmatrix} = E_k\left(\sum_{i=1}^{\infty}\chi_{ik}\Phi_i\right) . \tag{2.11}$$

Projecting the last equation on the electronic eigenfunction Φ_j,

$${\nabla_R}^2\chi_{jk} + \varepsilon_j\chi_{jk} + \sum_{i=1}^{\infty}\left(2\nabla_R\chi_{ik}\cdot\int\Phi_j^*\nabla_R\Phi_i d\mathbf{r} + \chi_{ik}\int\Phi_j^*\nabla_R^2\Phi_i d\mathbf{r}\right) = E_k\chi_{jk} . \tag{2.12}$$

The terms inside the summation correspond to the first and second coupling terms[23]. In the adiabatic approximation, the total wave function is restrained to one electronic potential energy surface and is justified when the system does not present radiation interactions and the energy levels are separated. This means that the diagonal terms in the integrals (i=j) are the only non-null terms (all others are equal to 0). Furthermore, the Born-Oppenheimer Approximation asserts that the resulting integrals can be neglected, considering that the movement of the ions is very slow with respect to the movement of the electrons. Then, replacing $\hat{T}_n$ in the equation 2.12,

$$(\hat{T}_n + \varepsilon_j(\mathbf{R}))\chi_{jk}(\mathbf{R}) = E_k\chi_{jk}(\mathbf{R}) . \tag{2.13}$$

This resulting equation and the eigenfunction equation (equation 2.4) allow computing the

dynamics of the ions and the electrons separately. In other words, the original problem is approximated in two simpler coupled problems: 1) to obtain the electronic solution with the nucleus positions as parameters and 2) to study the nucleus configuration properties using the electronic distribution as external potential. How to solve the coupled solution will be discussed in Section 2.2.5.

2.2.2 Electronic Problem Using Density Functional Theory

As mentioned before, the Born-Oppenheimer Approximation leads to the problem of solving an electronic Hamiltonian, defined in equation 2.4. This will be solved using the electronic density,

$$\rho(\mathbf{r}) = N_e \int \cdots \int |\Phi(\mathbf{r}, s_1, \mathbf{x}_2, ..., \mathbf{x}_{N_e})|^2 ds_1 d\mathbf{x}_2 \cdots d\mathbf{x}_{N_e} \,, \tag{2.14}$$

where $\mathbf{x}$ is formed by the electronic spin and coordinates. This function represents the spatial density of electrons in any state. Thus, the spatial integral of this function must yield the total number of electrons,

$$\int \rho(\mathbf{r}) d\mathbf{r} = N_e \,. \tag{2.15}$$

This is the main condition of the electronic density, and it will be a constraint for finding the solution for the electronic component.

2.2.3 Hohenberg-Kohn Theorems

In order to proceed to the electronic solution using the electronic density function, it is necessary to introduce two theorems known as the Hohenberg-Kohn Theorems[24]:

Theorem 1: The external potential is determined by the electron density. Namely, each electron density corresponds to a unique potential.

Theorem 2: For any trial density $\tilde{\rho}(\mathbf{r})$, such that $\tilde{\rho}(\mathbf{r}) \geq 0$ and $\int \tilde{\rho}(\mathbf{r}) d\mathbf{r} = N_e$,

$$E_0 < E[\tilde{\rho}] \,. \tag{2.16}$$

The proofs for these two theorems are very simple and can be found in several textbooks[22,23]. These theorems are important in this work, as they are the justification for using the density instead of the wave function of the system and they constitute the foundation of Density Functional Theory (DFT). The first theorem implies that ρ contains the information and capacity

to describe all the properties of the system. From the second theorem follows that the density can be found through the minimization of the functional of energy according to the variational principle. Namely,

$$\delta\left(E[\rho]-\mu\{\int\rho(\mathbf{r})d\mathbf{r}-N_e\}\right)=0\,, \tag{2.17}$$

where μ is a Lagrange multiplier that guarantees the constraint of equation 2.15. Solving this variation using the Euler-Lagrange equations yields

$$\mu=\frac{\delta E[\rho]}{\delta\rho}=v(\mathbf{r})+\frac{\delta F[\rho]}{\delta\rho(\mathbf{r})}\,, \tag{2.18}$$

with

$$F[\rho]=T[\rho]+v_{ee}[\rho]\,. \tag{2.19}$$

2.2.4 Kohn-Sham Equations

With the aim of obtaining a solution to the minimization problem, Walter Kohn and Lu Jeu Sham proposed a solution using an alternative artificial non-interacting system[25]. They considered the orbital states ψ_i, which are eigenfunctions of the density operator. Therefore, the electronic density for this system can be written in the spatial coordinates,

$$\rho(\mathbf{r})=\sum_i n_i\sum_s|\psi_i(\mathbf{r},s)|^2\,, \tag{2.20}$$

with n_i as the occupation number. Likewise, the kinetic energy of the artificial system in this basis set is

$$T[\rho]=\sum_i n_i\langle\psi_i|-\frac{1}{2}\nabla^2|\psi_i\rangle\,. \tag{2.21}$$

In general, for interacting systems, this expansion has an infinite number of terms. Kohn-Sham (KS) propose to consider a non-interacting system with a density equal to the density of the true system and under the influence of an effective potential. Since the KS system is defined to be at the ground state, then the minimization implies $n_i=1$ for all $i\leq N_e$, and $n_i=0$ otherwise. Then, equations 2.21 and 2.20 become

$$T_s[\rho]=\sum_{i=1}^{N_e}\langle\psi_i|-\frac{1}{2}\nabla^2|\psi_i\rangle\,, \tag{2.22}$$

$$\rho = \sum_{i=1}^{N_e} \sum_{s} |\psi_i(s, \mathbf{r})|^2 \ . \tag{2.23}$$

Note that this T_s would be the kinetic energy of the system if electrons did not interact. Thus, it is important to keep in mind that this term does not correspond to the interacting system. Instead, it is a completely arbitrary and auxiliary system for which the Hamiltonian can be constructed by adding a potential, v_s, without electron-electron repulsion and for which the ground-state electron density ρ is exactly that of the real system,

$$\hat{H}_s = -\sum_{i=1}^{N_e} \frac{1}{2}\nabla_i^2 + \sum_{i=1}^{N_e} v_s(r_i) \ . \tag{2.24}$$

For connecting this new system with the original one, the differences can be grouped in one term called the exchange-correlation functional,

$$E_{xc}[\rho] = T[\rho] - T_s[\rho] + v_{ee}[\rho] - J[\rho] \ , \tag{2.25}$$

where J is the Hartree functional. In this way, equation 2.19 is rewritten as

$$F[\rho] = T_s[\rho] + J[\rho] + E_{xc}[\rho] \ . \tag{2.26}$$

Replacing this result in the minimization equation yields

$$\mu = v_{eff}(\mathbf{r}) + \frac{\delta T_s}{\delta \rho} \ , \tag{2.27}$$

$$v_{eff} = v(\mathbf{r}) + \frac{\delta J[\rho]}{\delta \rho} + \frac{\delta E_{xc}}{\delta \rho} = v(\mathbf{r}) + \int \frac{\rho(\mathbf{r}')}{|\mathbf{r} - \mathbf{r}'|} d\mathbf{r} + v_{xc}(\mathbf{r}) \ . \tag{2.28}$$

Notice that equations 2.18 and 2.27 are equivalent. This equivalence means that Kohn and Sham reduced the original problem to a simpler one formed by non-interacting electrons affected by an effective potential v_{eff}. In other words, the electronic density of the system of interest can be obtained solving N one-electron equations

$$\hat{H}_{KS}\psi_i = \left[-\frac{1}{2}\nabla^2 + v_{eff}\right]\psi_i = \varepsilon_i \psi_i \ , \tag{2.29}$$

with

$$\rho(\mathbf{r}) = \sum_{i}^{N_e} \sum_{s} |\psi_i| \ . \tag{2.30}$$

Note that the potential v_{eff} depends on the density ρ, the density ρ on the KS orbitals ψ, and the orbitals ψ on the potential v_{eff}. Hence, equations 2.28, 2.29, and 2.30 must be solved self-consistently.

So far, the Kohn-Sham method consists in the introduction of a new non-interacting system with the same density without any approximation. However, it is necessary to consider that the exchange-correlation functional is unknown. As a consequence, a great part of the effort in DFT research has been devoted to propose exchange correlation functionals that are as precise and general as possible. Some examples of functionals are the local density approximation (LDA)[22], the Perdew-Burke-Ernzerhof (PBE)[26], among others[27]. Indeed, exchange-correlation functionals combine several exact constraints and corrections[28], and the election of the functional approximation is deeply dependent on the system, the planned type of computation, and the computational resources available.

2.2.5 Forces From Density

Finally, it is important to note that, with the ground-state electronic density of the system, it is possible to use the Hellmann-Feynmann theorem that relates the derivative of the total energy with respect to a parameter λ to the expected value of the derivative of the Hamiltonian with respect to the same parameter. This relation is[22]

$$\frac{dE}{d\lambda} = \langle \Phi_\lambda | \frac{\partial \hat{H}_e}{\partial \lambda} | \Phi_\lambda \rangle \ . \tag{2.31}$$

Thus, considering λ as the x Cartesian component of the position of the i-th atom, the Hellmann-Feynman theorem yields the x Cartesian component of the interatomic force (F^I) acting on the i-th atom. Applying this to the energy functional leads to[22]

$$F^I_{x_i} = \sum_{j \neq i} \frac{Z_i Z_j}{|\mathbf{R}_j - \mathbf{R}_i|^3}(x_j - x_i) - Z_i \int d\mathbf{r}' \rho(\mathbf{r}') \frac{x' - x_i}{|\mathbf{r}' - \mathbf{R}_i|^3} \ , \tag{2.32}$$

where Z is the atomic number and ρ is the electronic density obtained from DFT. Note that this force can be applied to simulate the classical evolution of the atoms of the system. This result will be used later in this work for simulating the evolution of the silver clusters and sampling different conformations, as explained in detail in the next section.

2.3 Quantum Mechanics/Molecular Mechanics (QM/MM)

In all real applications, there is an environment that could influence the physical properties of the system of interest. For some cases, the simulation of the isolated system, or in vacuum, could neglect important factors that affect the quality of the results. Computing forces that

consider the medium and the system of interest completely at the quantum level is too computationally expensive. To deal with this problem, Warshel and Levit proposed a method for mixing the advantages of quantum mechanics (QM) and molecular mechanics (MM)[29]. This method separates a smaller part of the complete system (CS), called the primary system (PS), and describes its electronic properties with quantum methods. The rest of the system, called the secondary system (SS), is simulated with classical approximations. Today, there are several QM/MM schemes that vary in how they describe PS-SS interactions. Currently, the most popular schemes are the subtractive and additive schemes.

In the subtractive scheme, CS interactions are computed classically, then, the classical energy of the PS is subtracted and replaced by a quantum energy. This implies that, in this scheme, the classical component does not affect the electronic distribution and the quantum component interacts classically with the rest of the system. In this scheme, the potential energy can be written as

$$E^{CS} = E^{PS+SS}_{MM} - E^{PS}_{MM} + E^{PS}_{QM}, \tag{2.33}$$

where the subscript and superscript indicate the approach and the region, respectively.

On the other hand, the additive scheme uses quantum approaches in the PS and classical approaches in the SS as independent systems, and adds an interaction potential between both. This is

$$E^{CS} = E^{SS}_{MM} + E^{PS}_{QM} + E^{PS|SS}_{QM/MM}, \tag{2.34}$$

where the last term is the interaction energy. This energy considers a hybrid electrostatic behavior defined by

$$E^{PS|SS}_{QM/MM} = -\sum_{i}^{N_{SS}} \int \frac{\rho(\mathbf{r}) q_i}{|\mathbf{r} - \mathbf{R}_i|} d\mathbf{r} + \sum_{i}^{N_{SS}} \sum_{j}^{N_{PS}} \frac{q_i Z_j}{|\mathbf{R}_i - \mathbf{R}_j|} + E_{NES}, \tag{2.35}$$

with $\rho(\mathbf{r})$ as the electronic density of the PS, $\mathbf{R}_i$ and q_i as the position and point charges of the SS atoms, Z_j as the atomic number of the PS atoms, and where E_{NES} contains the non-electrostatic electronic interactions.

Currently, there is not a predefined general procedure to compute E_{NES}, and it is usually defined ad-hoc as an LJ potential[30]. A way to describe E_{NES} is to replace equation 2.3 in equation 2.34, and approximate the energy of the complete system, E^{CS}, with a quantum approximation,

$$E_{NES} \approx E_{QM}^{CS} - E_{MM}^{SS} - E_{QM}^{PS} + \sum_{i}^{N_{SS}} \int \frac{\rho(\mathbf{r}) q_i}{|\mathbf{r} - \mathbf{R}_i|} d\mathbf{r} - \sum_{i}^{N_{SS}} \sum_{j}^{N_{PS}} \frac{q_i Z_j}{|\mathbf{R}_i - \mathbf{R}_j|} \,. \tag{2.36}$$

Then, this expression can be used to define the LJ parameters, fitting each interaction by pair type.

To apply QM/MM, we must define crucial aspects such as the border between the quantum and classical component[31,32] or the interaction potentials between the PS and SS, which could require ad-hoc corrections[33,34]. These definitions depend on, for example, the existence of covalent bonds between atoms of both regions or the basis set's accuracy in describing the electronic distribution of the PS. A correct definition of these aspects could avoid typical errors, such as the "electron spill out" problem[35]. A complete explanation of these problems and their solutions is beyond the scope of this introduction, but it is discussed elsewhere[36,37,30].

2.4 Statistical Aspects

It is well known in statistical mechanics that the probability of finding a configuration of a canonical ensemble is described via the Boltzmann factor[38],

$$p(\mathbf{R}) \;\; = Z^{-1} \;\; e^{-\frac{V(\mathbf{R})}{k_B T}} \,, \tag{2.37}$$

where $\mathbf{R}$ is a multidimensional vector that contains the coordinates of the N_a particles of the system, (namely $\mathbf{R} = (\mathbf{R}_1, ..., \mathbf{R}_N)$), $V(\mathbf{R})$ is the potential energy of the configuration, k_B is the Boltzmann constant, T is the temperature of the system, and Z is a normalization factor.

This expression for probability is the central object of statistical mechanics, as the mean value of an observable, g, can be obtained by

$$\langle g \rangle = \int_{-\infty}^{\infty} d\mathbf{R}\, g(\mathbf{R}) p(\mathbf{R}) \,. \tag{2.38}$$

In this work, we are specifically interested in studying configurations with common properties. Therefore, we define a state as the set of configurations that belong to the same basin in the potential energy landscape. In this sense, each state has an associated hypervolume. Thus, the probability of finding the system in one state is the same as the probability of finding the system in one of the configurations of that hypervolume, that is,

$$P_A = Z^{-1} \int_{V_A} d\mathbf{R}\, e^{-\frac{V(\mathbf{R})}{k_B T}} \,, \tag{2.39}$$

where A refers to the particular state.

From a statistical point of view, the free energy of one state A is defined as the quantity that replaces the energy in the Boltzmann factor to describe the probability of finding the system in said state,

$$e^{-\frac{F_A}{k_B T}} = P_A \, . \tag{2.40}$$

Likewise, the free-energy surface (FES), or the potential of mean force (PMF), is defined as the function of a set of variables $s = S(\mathbf{R})$ that replaces the potential energy in the Boltzmann factor to describe the projection of the probability in that set of variables,

$$e^{-\frac{F(s)}{k_B T}} = P(s) = \frac{Z^{-1} \int d\mathbf{R} \delta(s - S(\mathbf{R})) e^{-V(\mathbf{R})/k_B T}}{\eta^{uni}(s)} \, , \tag{2.41}$$

where $\eta^{uni}(s)$ is a scale function, necessary for conserving the norm, the units, and the properties of the Dirac delta function. In order to obtain relevant information on the states of the system, the variables s, also called Collective Variables (CVs), are chosen in such a way that the hypervolumes that define states in coordinate space can be separated into hypervolumes $\tilde{V}$ in the space of s variables. If the s variables fulfill this property, the probability of one state can be obtained from the free-energy surface as

$$P_A = \int_{\tilde{V}_A} e^{-\frac{F(s)}{k_B T}} ds = Z^{-1} \int_{V_A} d\mathbf{R} \, e^{-\frac{V(\mathbf{R})}{k_B T}} \, . \tag{2.42}$$

Analytic integration of this equation is not possible in most cases because (for most cases) there is not an analytic expression for the potential energy. Therefore, it is necessary to consider other alternatives to extract this information.

2.5 Simulations and Sampling

An approximation of the probability distribution of an ensemble can be achieved if the system is ergodic. This means, if the average of an observable over an ensemble coincides with the average over time[39]. We consider that the probability of finding a configuration of the system in a set of copies is the same as the probability of finding said configuration in a simulated time evolution of a single copy[40].

With this in mind, we will reconstruct the probability distribution of equation 2.37 simulating the evolution of the system over a large time lapse conserving the number of particles, volume, and temperature (NVT ensemble). The basis to simulate the evolution of an atomic

system is using Newton's equation,

$$m_i \frac{d^2\mathbf{R}_i}{dt^2} = \mathbf{F}_i \,, \tag{2.43}$$

where $\mathbf{F}_i$ and m_i are the net force and the mass of the i-th atom, respectively. In a completely classic simulation, the forces are the negative of the gradient of the potential energy approximated with analytic functions. If the electronic distribution is considered, the force used in this equation corresponds to the result of the Hellmann-Feynmann theorem (equation 2.32).

Since Newton's equation conserves the energy and not the temperature of the system, we have to couple the system with a heat bath in order to obtain the expected distribution. The condition for defining this coupling is given by the equipartition theorem that relates the temperature with the kinetic energy of the system[41]

$$E_K = \frac{n_{dof}}{2} k_B T \,, \tag{2.44}$$

where n_{dof} is the number of degrees of freedom of the system. We add terms to the equations of motions to regulate the temperature. Langevin dynamics, for example, add a friction term and a fluctuating force[42],

$$m_i \frac{d^2\mathbf{R}_i}{dt^2} = \mathbf{F_i} - \eta m_i \frac{d\mathbf{R}_i}{dt} + \sqrt{2 m_i \eta k_B T}\, \xi(t) ds \,, \tag{2.45}$$

where η is the damping constant and $\xi(t)$ is a white Gaussian noise.

Another way to introduce a coupling with a heat bath is to use the Berendsen thermostat[43]. This thermostat rescales the velocities multiplying by the factor

$$\chi = \left(1 + \frac{dt}{\tau_t}\left(\frac{T_d}{T_r} - 1\right)\right)^{1/2} \,, \tag{2.46}$$

where T_d is the target temperature for the simulation, T_r is the temperature of the system (computed using equation 2.44), and τ_t is a parameter defined by the user that controls the strength of the coupling. Note that if the computed temperature is greater than the target value, this factor would be lower than one, which would lead the temperature of the system to decrease. In the opposite case, the effect of the thermostat is to increase the magnitude of the velocities when the temperature is lower than the target value. Note that this thermostat does not strictly describe a canonical distribution of the velocities in equilibrium. However, in practice, it is widely used because it has the advantage of quickly equilibrating the system, and it gives an approximate description for systems with a large number of particles and also

provides a proper election of the coupling strength with the bath[44].

In this way, we can simulate the evolution of the system during a time lapse that should be enough to obtain a reconstruction of the probability from a normalized histogram of the explored configuration landscape. However, a complete exploration is sometimes computationally impossible to achieve when the energetic barriers between states is high in relation to the thermal energy. For these cases, the transition from one state to another is called a rare event[45]. In other words, the probability of observing a transition is low for these systems, and a complete exploration of the configuration landscape would take much more time than what is possible to simulate computationally with the currently available resources, even with the most advanced supercomputers.

For that reason, several methods have been proposed to overcome this limitation. In the literature, these methods are referred to as enhanced sampling methods and include techniques like Umbrella sampling[46], Replica exchange[47], and Metadynamics[8]. A complete explanation of each one of those methods is beyond the interest of this work, but there are detailed reviews with further explanations[48,49]. In this work, we focus our attention on Metadynamics.

2.5.1 Collective Variables

For large systems, it is difficult to extract clear information by monitoring the coordinates of all the atoms. Instead, it is possible to simplify the monitoring by defining functions of coordinates that describe the chemical properties that we are interested in. Those functions are called Collective Variables (CVs). These can also be used for biasing specific degrees of freedom or analyzing how the system evolves. In other words, CVs project the multi-dimensional system onto a small set of relevant and interpretative degrees of freedom.

A careful election of collective variables is crucial for achieving a proper analysis or an adequate acceleration of the degrees of freedom in enhanced sampling methods. Although there is no direct recipe for constructing CVs, some important characteristics have been defined[50]:

- They should differentiate the relevant states of the system, including the stable states and the intermediate states.
- They should include the slow modes of the system.
- They should be as limited in number as possible.

The first condition is essential because it guarantees the physical meaning of the CVs and enables a description of the evolution of the system along continuous reaction paths. For enhanced sampling methods that bias these degrees of freedom, this property is necessary to push the system along that path.

The second condition implicitly contains an idea behind the election of the CVs: that there are fast degrees of freedom, which can be rapidly averaged along slow variables. This is analogous to the adiabatic approximation. Basically, this is another way to say that CVs should contain the relevant degrees of freedom of the system.

Last but not least, the number of CVs should be small to allow for interpretability. Considering many collective variables implies a larger space to be explored. This is a practical limitation in the sense that a larger space needs more computational time. Additionally, analyzing a high dimensional set of CVs is far from simple, which contradicts one of the motivations for using CVs. In most of the literature related with the implementation of CVs, the number is lower than 4 [50,18,51,7].

2.5.2 Metadynamics

Metadynamics (MTD)? is a method that adds a history-dependent bias potential over a small set of CVs, $\mathbf{s}$. Typically, the bias is accumulated as a sum of Gaussians centered along the CV trajectory, namely in the values of the CVs of previous steps. This pushes the system to explore different configurations and enhances the sampling. In particular, in Well-Tempered Metadynamics (WT-MTD)[52] the bias potential at time t is

$$V_B(\mathbf{s},t) = \sum_{t'=\tau,2\tau,\ldots}^{t'<t} We^{-\frac{\beta\, V_B(\mathbf{s},\, t')}{\gamma}}\, e^{-\sum_i \frac{[s_i\, -\, s_i(t')]^2}{2\sigma_i}}\,, \tag{2.47}$$

where W is the initial height of the bias, τ is the time-lapse to add a new term to the summation in the bias potential, β is the inverse of k_BT, γ is a bias factor, and σ_i is the width of the Gaussians. Note that the first exponential decreases the height of the deposited Gaussians where previous bias energy has been added. This reduction of height of the new Gaussians reduces the error and avoids exploration towards high free-energy states that are thermodynamically irrelevant. The bias factor γ regulates the rate in which the magnitude of the new added bias decreases: the lower the bias factor, the faster the decrease. The last exponential is a multiplication of Gaussians in the direction of CV i with width σ_i centered at the CV value at time t'. In this way, the system is forced to explore different conformations.

With this additional biasing potential, the net atomic force $\mathbf{F}_i$ (equation 2.45) becomes

$$\mathbf{F}_i = \mathbf{F}_i^I - \left.\frac{\partial V_B(\mathbf{s},t)}{\partial \mathbf{s}}\right|_{\mathbf{s}=\mathbf{s}(t)} \left.\frac{\partial \mathbf{s}(\mathbf{R})}{\partial \mathbf{R_i}}\right|_{\mathbf{R}=\mathbf{R}(t)}\,, \tag{2.48}$$

where $\mathbf{F}^I$ represents the interatomic forces presented in equation 2.32.

The main advantage of this method is that it allows obtaining an estimation for the FES. In

particular, for WT-MTD, it is proved that[9]

$$\lim_{t\to\infty} V_B(\mathbf{s}, t) = -\frac{(\gamma - 1)}{\gamma} F(\mathbf{s}) \,. \tag{2.49}$$

In short, the energy added in MTD pushes the system to explore different conformations, and that additional energy converges to the free-energy surface of the system.

3

Development of the ASE-PLUMED interface

3.1 Summary

In this chapter, we present details about the codes used and developed in this work. We start with the Atomic Simulation Environment (ASE), which allows integrating several of the most popular atomistic simulation codes to perform MD simulations. One of those codes is GPAW, that implements DFT, efficiently removing strong oscillations from the wave functions close to the nucleus and expanding the smoothed wave functions in a different basis set. We also present the PLUMED plug-in, a code specialized in the computation of collective variables and the application of enhanced sampling algorithms. Prior to this thesis, it was not possible to use PLUMED with ASE, but in this work, we created the ASE-PLUMED interface, which is an ASE object-denoted calculator. In our notation, Plumed is the ASE calculator and PLUMED is the plug-in. At each time step, PLUMED receives the information of the system configuration and sums the biased and unbiased energies, calculating the forces for the next integration. We present the details of this interface and the tests to prove that it works properly. Due to the object-oriented structure of ASE, this calculator can work as an interface to all codes integrated in ASE. This enables carrying out *ab-initio* enhanced sampling algorithms.

3.2 ASE

Atomic Simulation Environment[53] (ASE) is an open-source code written in Python, with an object-oriented structure that allows setting, manipulating, and running atomistic simulations. A central *Atoms* object contains the information of the system, including the chemical symbols of the atoms, a simulation cell, the positions of the atoms, their velocities, among others.

The *Atoms* object has a calculator attached, which contains methods to compute specific properties of the system. Typically, the calculator computes the potential energy and forces according to the description level. Special calculators can compute specific properties, such as electronic distribution or dipole moments. An advantage of the object-oriented structure is that the user can select this calculator without changing the structure of the code. The selected calculator can be standalone or an interface to one of the many widely used quantum and classical atomistic simulation codes. Some examples of the implemented calculators that work along with ASE are Gaussian[54], CP2K[55], gromacs[56], lammps[57] and GPAW[58]. The last one is a DFT calculator that will be used in our simulations.

In addition to visualization tools, ASE has many methods for studying changes to the physical properties of the atomic systems based on the calculation of forces and energies. Some of them are optimization, nudged elastic band and molecular dynamics algorithms. Berendsen and Langevin dynamics are among the molecular dynamics algorithms included in ASE. These algorithms numerically solve the equations described in Section 2.5 via time discretization using the Verlet integrator. Thus, it is possible to simulate the evolution of the system and its properties.

3.3 GPAW

GPAW[58] is a DFT Python code, especially designed for working as a calculator in ASE. This code is based on the projector-augmented wave (PAW) method[59] that deals with the problem of strong oscillations of the all-electron wave function near the nucleus. This is a serious problem because it is difficult to obtain convergence in those regions, unless we define a grid spacing tiny enough to differentiate those changes or a large basis expansion, depending on the basis set. Of course, these options are time and memory consuming. Thus, the solution proposed in the PAW method is to seek a linear operator, $\mathcal{T}$, which generates the original orbitals of the Kohn-Sham equation by acting over a smoother function, that is

$$|\psi_n\rangle = \mathcal{T}|\tilde{\psi}_n\rangle \,, \tag{3.1}$$

where $|\psi_n\rangle$ is the original wave function and $|\tilde{\psi}_n\rangle$ is the auxiliary smoother function, known as pseudo wave function. As the condition of smoothness applies for conditions close to each nucleus, we define $\mathcal{T}$ as

$$\mathcal{T} = 1 + \sum_i \mathcal{T}^i \,, \tag{3.2}$$

where $\mathcal{T}^i$ is different from the null operator only in the region inside a radius r_i around the atom i. Using equation 3.1 in the Khon-Sham equation (equation 2.29),

$$\mathcal{T}^\dagger H_{KS} \mathcal{T} |\tilde{\psi}_i\rangle = \varepsilon_i \mathcal{T}^\dagger \mathcal{T} |\tilde{\psi}_i\rangle \tag{3.3}$$

GPAW has implemented three bases for expanding the pseudo wave functions[60]:

- Grid or finite differences (fd): the pseudo wave function is

  $$\tilde{\psi}_i(\mathbf{r}) = \tilde{\psi}_i(ih, jh, kh) \,,$$

  with h being the grid spacing, and (i, j, k) the indices of the grid points.

- Plane Waves (PW): the pseudo wave function is defined as an expansion of plane waves until a cutoff energy, E_c,

  $$\tilde{\psi}_i(\mathbf{r}) = \sum_{G^2/2 < E_c} c_G e^{i\mathbf{G}\cdot\mathbf{r}} \,.$$

- Localized atomic orbitals (LCAO)[61]: the pseudo wave functions are expanded onto a set of atomic-like orbitals

  $$\tilde{\psi}_i(\mathbf{r}) = \sum_{anml} c_{inml} \mathcal{R}_{nl}(r^a) Y_{ml}(\hat{\mathbf{r}}^a) \,,$$

  where $\mathcal{R}_{nl}$ and Y_{ml} are atomic radial functions and spherical harmonics, while $\mathbf{r}^a$ is the distance from $\mathbf{r}$ to the nucleus a, $\mathbf{r}^a = \mathbf{R}^a - \mathbf{r}$.

These three options allow finding numerical solutions to the electronic density, avoiding the problem of strong oscillations close to the nucleus of the system under the PAW scheme. The LCAO basis set is the fastest and has the lowest memory consumption, in exchange for loss of precision[61,58]. The grid basis consumes more memory than the others[58]. PW is faster than the grid basis in small systems, but, in large systems, the grid basis parallelizes better than PW[58]. The grid basis and PW can achieve the same level of precision, varying the cutoff energy and the grid spacing, respectively[58].

In order to visualize the performance of this method, we present the case of a CO molecule taken from GPAW documentation. For this example, we fix the C atom at -0.6 Å and the O

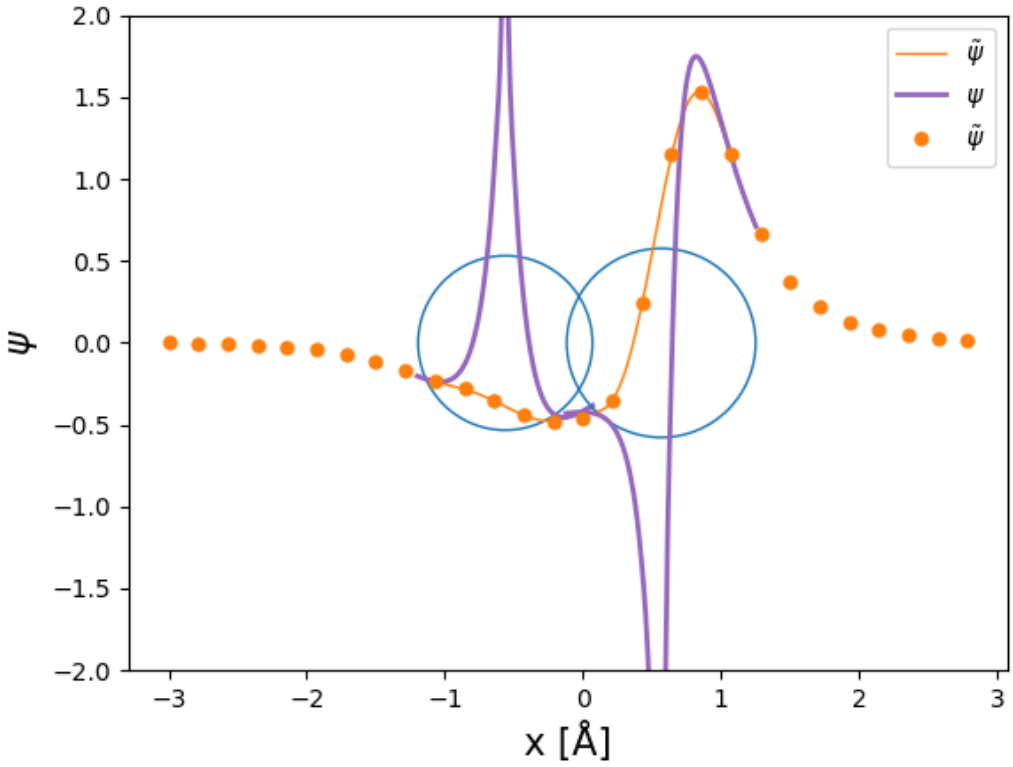

Figure 3.1: Comparison of the pseudo wave function ($\hat{\psi}$, orange solid line) and the real wave function (ψ, purple solid line) inside a cutoff radius along the x-axis for the CO case study. Dots show the resulting wave function in the entire space space using LCAO. Blue circumferences represent the cutoff radius around each atom.

atom at 0.6 Å of the x-axis. Figure 3.1 shows a comparison of the real and the pseudo wave functions along the x-axis. It is clear that there is a considerable difference between using a complete description (abrupt changes) versus the implemented PAW method (smooth). Note that the self consistence convergence is harder to obtain for the real wave function inside the cutoff radius, and that outside the cutoff radius, both wave functions are equal.

3.4 PLUMED

PLUMED[62] is an open-source code, written in C and C++ with a wrap for Python in the latest releases (since version 2.5). This library includes different tools for implementing enhanced sampling algorithms, free-energy methods and it is useful in post-processing simulated tra-

jectories.

Among the advantages of PLUMED is the large set of collective variables that are widely used by the community of molecular simulations. Moreover, PLUMED developers are constantly adding new collective variables and new enhanced sampling methods for better description of the systems.

PLUMED is mainly used as a plug-in, which works along with MD codes. Some MD codes that are already patched with PLUMED are ACEMD, Amber, Gromacs[56], CP2K[55], among others. Figure 3.2 shows the general interaction of this plug-in with an MD engine. Note that the MD code actually controls the execution of all PLUMED actions. The first step is to initialize the MD functions, atom positions, and velocities; then, the PLUMED object is initialized with the specific details of the systems, like the number of atoms and the size of the time step. In the initialization step, PLUMED reads the actions that must be executed during the simulation: computing CVs, adding bias potential, etc. The MD code solves the equation of movement (equation 2.45) for each time step and sends the changes to PLUMED. For MD, PLUMED executes its actions and returns the forces, and the MD code reintegrates the following time step changes.

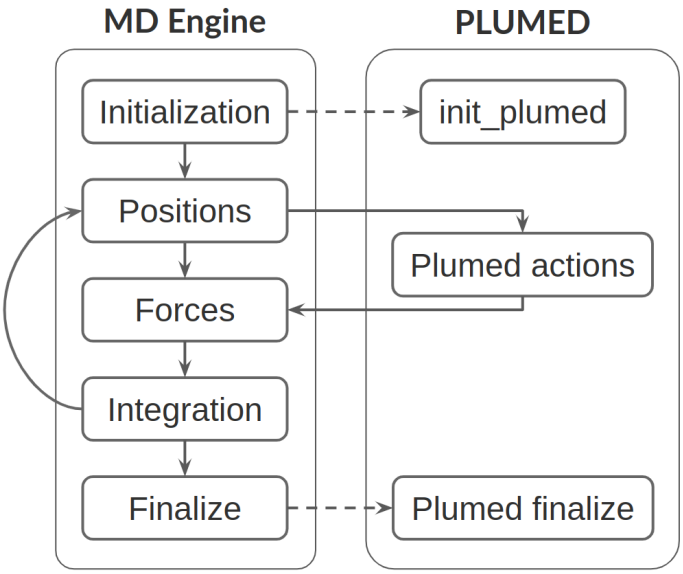

Figure 3.2: Diagram of the general workflow of the PLUMED plug-in with a molecular dynamics code. Reprinted figure with permission from[62].

3.5 Result: Interface

One of the achieved objectives of this work was to create an interface between PLUMED (>= version 2.5) and ASE (version > 3.22.1). This was developed to have the possibility of using the methods implemented in PLUMED within ASE, and vice versa. In this way, both communities (ASE and PLUMED users) gain a benefit from this development. Appendix B contains the created patch that works as an ASE calculator (that we called Plumed). In this section, we explain how it works and provide important details and tests that prove that our development works properly.

Our patch has slight differences compared to PLUMED interfaces with other MD codes, as ours uses PLUMED's wrap for Python. One difference is that Plumed reads the actions –such as computing CVs or adding bias– directly from the MD code, while in other patches, PLUMED actions are defined in an external file. Moreover, Plumed actions are not parallelizable but are initialized only in the master process (usually rank=0) that executes and sends the bias forces to the slave processes during the simulation. This is important because PLUMED always creates output files, and an initialization from all processes would imply as much output files as the number of processes, all of them with the same information. In this way, parallelization is completely invested in the computation of MD forces which, in the *ab-initio* case, represents the most resource-consuming part.

The key points for the correct behavior of the interface are the horizontal arrows that connect both codes in Figure 3.2. To start, Plumed receives the *Atoms* object as its arguments, a list of strings with orders for the PLUMED set-up, a calculator for computing the unbiased forces, and the magnitude of the time step in the simulation. Considering that PLUMED units are different than ASE units (Table 3.1), we added the transformation rules to the Plumed calculator. In the initialization, Plumed uses the information contained in the *Atoms* object, such as the number of atoms and the simulation cell (when the *Atoms* object has a defined cell, Plumed assumes periodic boundary conditions unless specified otherwise in the setup list). At each time step, ASE calls Plumed methods to compute forces and energies, and Plumed provides PLUMED the *Atoms* data –positions, unbiased potential energy, and charges– and receives the bias forces and energies. Finally, Plumed adds the energy and bias forces to the unbiased energy and forces.

This interface was added to the development version of ASE after discussions with the developers regarding the specific code structure of this package. We included a tutorial that is now in the ASE documentation and which guides the user in the execution of the test shown in the following section (https://databases.fysik.dtu.dk/ase/ase/calculators/plumed.html).

3.5.1 Validation tests

As an accuracy test for our new Plumed calculator and as a user guide, we used a tutorial from the PLUMED documentation [62] as a benchmark system. This consists of a WT-MTD/Langevin simulation for a simple system formed by seven artificial atoms (mass=1 in Lennard Jones units) with Lennard-Jones (LJ) interactions in a planar space starting from the configuration of minimum energy (first configuration at left in Fig. 3.3). The LJ cluster has several stable isomers (Figure 3.3), which can be distinguished in a space of the CVs' second and third central moments of distribution of coordination numbers (labeled as SCM and TCM, respectively second central moment and third central moment). The nth central moment μ_n of the N_a atoms cluster is defined as

$$\mu_n = \frac{1}{N_a} \sum_{i=1}^{N_a} (X_i - \langle X \rangle)^n \ , \tag{3.4}$$

where X_i is the coordination number of the i-th atom,

$$X_i = \sum_{i \neq j} \frac{1 - (R_{ij}/d)^8}{1 - (R_{ij}/d)^{16}} \ . \tag{3.5}$$

We used LJ dimensionless reduced units. The parameters of the simulation are $d = 1.5$, $k_B T = 0.1$, friction coefficient fixed equal to 1, initial bias height of 0.05, Gaussians width of 0.1 (for both CVs), and a bias factor of 5.

For this system, we compared the free energy obtained by PLUMED as a standalone code and the free energy estimated when using our new Plumed calculator that adds a bias force to an LJ-force calculator in ASE. For both cases, we ran 121 trajectories starting from the same configuration. In Figure 3.4 (a) and (b), we show the average free-energy surface as a function of the two CVs for the new Plumed calculator and PLUMED alone, respectively.

Table 3.1: Comparison between PLUMED and ASE units.

	PLUMED	**ASE**
Energy	kJ/mol	eV
Length	nm	Å
Time	ps	$\text{Å}\sqrt{\text{amu/eV}}$
Charge	e	e
Mass	amu	amu

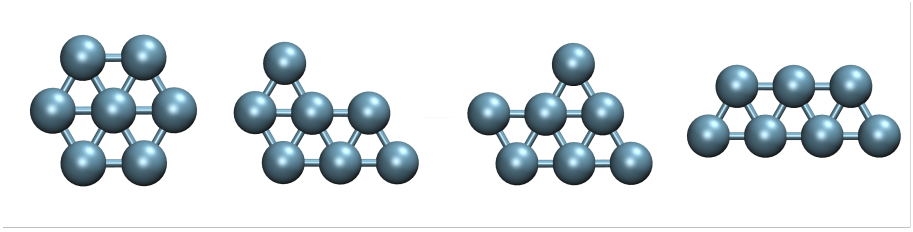

Figure 3.3: Stable isomers of the LJ-planar system

The free-energy error is the standard error of the 121 replicas (*i.e., the standard deviation over the square root of the number of simulations*). These are shown in 3.4 (c) and (d). The results show that the Plumed calculator performs well, since its average free-energy landscape converges to the same values (within error) as the results from standalone PLUMED. The differences between PLUMED and ASE-Plumed –for example, different random number generators– can be seen as a different pattern of errors in the figure. However, the error range is equal between both codes, as expected.

Apart from this proof, we added two tests (Appendix C) to the ASE source code (https://gitlab.com/ase/ase/-/blob/master/ase/test/calculator/plumed/test_plumed.py) to ensure an alert error will be raised in case any change to ASE or PLUMED generates incompatibilities with the actual interface. Short runs of at most 60 steps support these tests, which consider:

- Units: Table 3.1 shows the current relation between ASE and PLUMED units. If something in that table changes, one of the tests will fail.
- CV computation: we included computation of very simple CVs (distance-related) in order to verify that ASE sends data to PLUMED correctly.
- Bias forces: a short MTD with NVE simulation tests that the forces received from PLUMED are correct.
- Restart: one of the tests splits a simple MTD simulation of 60 steps into two 30-step parts to check for proper behavior on restart.

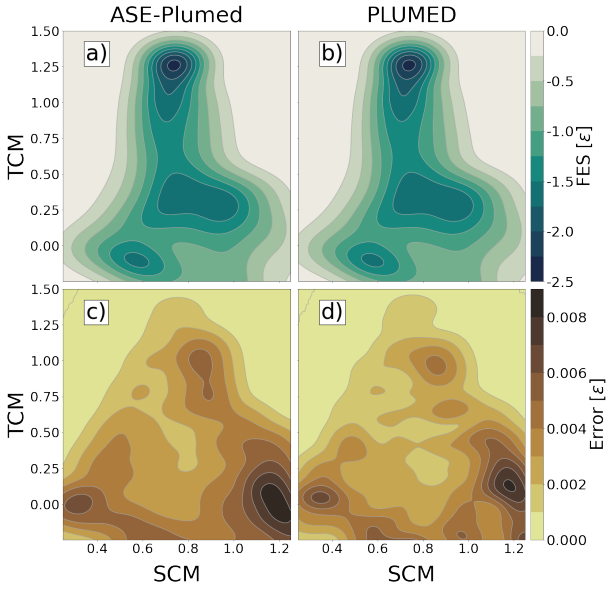

Figure 3.4: Comparison of the free-energy landscape of seven atoms with Lennard-Jones interactions for standalone PLUMED and the new ASE-Plumed calculator using WT-MTD in the space of second central moment (SCM) and third central moment (TCM). (a) and (b) are the averaged free-energy landscapes in energy LJ units, over 121 trajectories, as function of the CVs' second and third central moments of distribution of coordination numbers. The standard error of the free-energy landscapes is shown in (c) and (d) for the ASE-Plumed interface and PLUMED, respectively.

4

Free-energy landscapes of ultrasmall silver clusters

4.1 Summary

In this chapter, we study small silver clusters using the Plumed interface described in the previous chapter. In particular, we extract the free-energy surface of Ag_5 and Ag_6 in gas phase (in vacuum) and Ag_2 embedded in water solution. We first discuss a few experimental and computational results in order to choose the DFT set up. After that, we detail the selection of the collective variables and WT-MTD parameters based on molecular dynamics simulations. Finally, we present the estimated free-energy surfaces for these systems found by implementing WT-MTD at different temperatures.

4.2 DFT parameters

Small neutral silver clusters have planar low-energy isomers, and as the number of atoms increases, the 3D isomers get closer in energy to the lowest energy isomer until Ag_7, where the trend changes and the lowest energy configuration is a 3D structure[4,5].

In the case of the Ag_5 cluster, experimental studies with Raman and optical photoabsorption spectroscopy agree that the lowest energy isomer of this system has a planar trapezoidal shape[63]. Ag_5 isomers have been studied through computational methods such as Hartree-

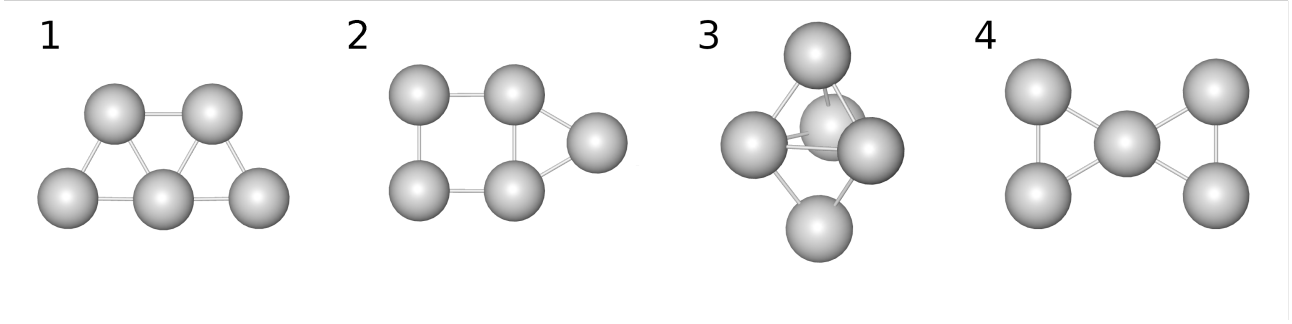

Figure 4.1: Isomers of the Ag_5 cluster. 1) trapezoid, 2) edge-capped, 3) bipyramidal, and 4) bow-tie.

Fock, coupled-cluster CCSD(T) and Density Functional Theory (DFT)[64,4,5]. All computational methods predict a 3D bipyramidal isomer about 0.4-0.5 eV higher in energy than the lowest energy state. Various methods predict other planar isomers with energies that are more strongly method-dependent. PBE, N12, and TPSS exchange-corrrelation functionals predict a planar isomer (edge-capped square) between the trapezoid isomer and the three-dimensional bipyramidal isomer. However, this is not found with the CCSD(T) method. Moreover, with the CCSD(T) method, a planar isomer denoted bow-tie is found[5] at the same energy of the three-dimensional isomer, but other DFT functionals, like PBE and N12, place bow-tie isomer energy 0.2-0.3 eV below the three-dimensional bipyramidal isomer energy[4]. In Fig. 4.1, the lowest isomer in energy –trapezoidal isomer– is isomer 1 and the 3D bipyramidal is represented as isomer 3. The edge-capped square isomer is isomer 2 in Fig. 4.1. The bow-tie isomer is isomer 4 in Fig. 4.1.

So far, there is not a general agreement regarding the driving force that keeps planar configurations stable. However, some authors have suggested theoretical explanations related with electronic interactions. Ferrighi et al., for example, studied the 2D-3D transition for cationic and anionic gold clusters with different functionals and obtained different number of atoms in clusters for 2D-3D transition[65]. They mention that correlation energy favors the stability of 3D structures and kinetic energy make the 2D structures more stable. In agreement with this explanation, they obtained a transition to 3D structures with lower number of atoms in clusters for exchange-correlation functional with smaller kinetic energy corrections. On the other hand, other authors have observed a stabilization of 3D golden clusters due to van der Walls corrections in the exchange correlation and thermal effects[7]. In this sense, we obtain similar results for Ag_6 clusters, for which, we predict a stabilization of the 3D configurations when we consider thermal effects at 300K.

Likewise, the Ag_6 cluster has been studied experimentally and computationally using the DFT[4] and CCSD(T) methods[5]. All computational methods suggest a triangular-planar isomer as the configuration of minimum energy, followed by a 3D pyramidal isomer, with a differ-

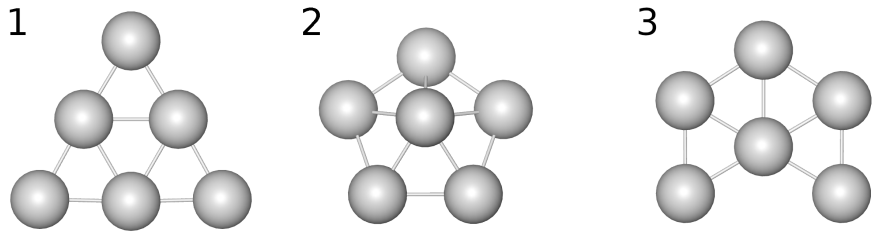

Figure 4.2: Isomers of the Ag_6 cluster. 1) triangular, 2) pyramidal and 3) incomplete hexagon.

ence of energy of 0.1-0.2 eV. A third isomer (planar incomplete hexagon) is predicted with an energy of 0.3 eV with respect to the minimum energy configuration. Absorption spectrum experiments suggest a possible mixture of triangular and pyramidal isomers, although the difference in energies makes the presence of the pyramidal isomer not truly favorable according to the zero energy analysis[66,3]. Figure 4.2 shows the Ag_6 isomers: the lowest in energy, the triangular isomer, labeled as isomer 1; the next stable configuration, the 3D pyramidal, labeled as isomer 2; and as isomer 3, the incomplete hexagon.

Table 4.1 summarizes the potential energies of all isomers discussed in this section. Chen et. al.[5] computed the CCSD(T) energies after optimizing at the B3LYP/aD level (column CCSD(T)). Duanmu and Truhlar[4] optimized the isomers with N12/jun-cc-pVTZ-PP, and then computed the energies with the same functional and basis (column N12). We optimized each structure using PBE and TPSS functionals with the grid basis and PBE with the LCAO basis, and then calculated the energies at the same level (PBE, TPSS, and PBE-LCAO-PVAL columns).

By comparing the Ag_5 PBE and CCSD(T) columns, we can observe that PBE provides an overestimation of the 2D-3D energy difference by about 0.1 eV (row 3), which is reduced through the use of the p-valence basis. On the contrary, for Ag_6, DFT-PBE gives a good estimation of the 2D-3D energy difference (row 6), which is then underestimated once the LCAO p-valence replaces the finite-difference method. This result would point to the PBE delocalization of electronic density, which is then slightly corrected by the use of the localized atomic LCAO p-valence basis, but such cancellation is only beneficial in the case of Ag_5.

In the TPSS column of Table 4.1, we report optimization of isomers with the TPSS exchange-correlation functional and finite difference basis. As reported earlier for gold clusters[65], this functional yields a good accuracy and reproduces the order and energies of CCSD(T) calculations. We suggest its use in future simulations, although it was out of reach for the computational resources used in this work. Here, we used the PBE exchange-correlation functional with the LCAO basis, which efficiently provides the correct 2D-3D ordering.

We proceed to apply WT-MTD to our systems of interest in order to take into account variations due to entropic effects.

Table 4.1: Silver cluster isomer energies in eV relative to the lowest isomer using different methods. We include energies obtained with the coupled cluster method and with DFT functionals like N12, PBE, and TPSS. With the functional PBE, we also include the predicted energies with the faster LCAO p-valence basis used in this work.

System	Isomer	Symmetry	Dimension	CCSD(T)[5]	N12[4]	PBE	PBE LCAO PVAL	TPSS
Ag_5	1	C_{2v}	2	0	0	0	0	0
	2	C_{2v}	2	-	0.27	0.22	0.26	0.27
	3	C_{2v}	3	0.43	0.53	0.55	0.40	0.46
	4	D_{2h}	2	0.46	0.36	0.39	0.53	0.43
Ag_6	1	D_{3h}	2	0	0	0	0	0
	2	C_{5v}	3	0.20	0.25	0.23	0.09	0.21
	3	C_{2v}	2	0.30	0.29	0.28	0.27	0.28

4.3 Selection of collective variables

As mentioned previously in the theory section, selecting CVs is not trivial in the implementation of enhanced sampling methods such as as MTD and its variations. Unfortunately, there is not an automatic mechanism to select the set of CVs, although some researchers have reported some advances in this regard[67,68,69]. Our first task was to find a set of CVs with the proper behavior to describe the states of the system, for which we explored several sets.

One of the CVs we considered measured the distance to the stable isomers for Ag_5. To this end, we used the root-mean-square deviation (RMSD) of the inter-atomic distances,

$$RMSD(\mathbf{R};\mathbf{R}^{ref}) = \sqrt{\frac{1}{N_a(N_a-1)}\sum_{i\neq j}[d(\mathbf{R}_i,\mathbf{R}_j) - 0.1\,d(\mathbf{R}_i^{ref},\mathbf{R}_j^{ref})]^2}\,, \tag{4.1}$$

where $\mathbf{R}^{ref}$ corresponds to the coordinates of the atoms of the reference configuration. In our case, we used isomers 1 and 3 in Figure 4.1 as reference configurations. In this way, we had two CVs corresponding to the RMSD for the trapezoidal and the bipyramidal isomer. From the first tests, we noticed that these CVs were inversely proportional: when one of them increased, the other decreased at the same rate. Hence, we selected the CV_{RMSD}, a linear combination of both RMSD distances,

$$CV_{RMSD} = \frac{1}{2}\left[RMSD(\mathbf{R};\mathbf{R}^{isomer_1}) + RMSD(\mathbf{R};\mathbf{R}^{isomer_3})\right]\,. \tag{4.2}$$

We implemented MTD using CV_{RMSD} and fixed the height of the Gaussians to 0.1 eV and the

width to 0.2 Å. Figure 4.3 shows CV_{RMSD} as a function of time. Analyzing these trajectories, we realized that this CV pushes the system towards high-energy states (thermodynamically irrelevant) as shown in the top of the image. Moreover, these transitions (via very high-energy transition states) frequently interchanged atoms, generating different values of the CV although the configuration was already the same. This is due to the symmetry of interchange defined in the RMSD. For this reason, we discarded the use of these CVs.

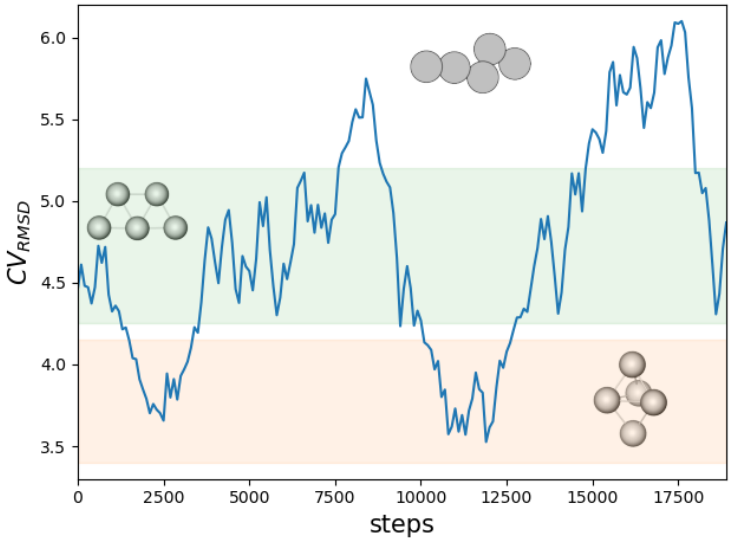

Figure 4.3: Evolution of the CV_{RMSD} defined in equation 4.2 in MTD simulation. Green and red shadow zone represents the values of the CV that corresponds to the isomer 1 and 2, presented in Fig. 4.1. The isomer is an example of a high energy configuration.

We also considered the CV coordination number C and radius of gyration R, which were previously used for studying the conformations of the Au_{12} cluster[19]. The coordination number is

$$C = \sum_{i=1}^{N_a} X_i, \tag{4.3}$$

where X_i is defined in equation 3.5 and the reference distance d was set to 2.8Å to include all first neighbor distances in the silver isomers. This CV measures the number of bonds in the system. The radius of gyration is

$$R = \left(\frac{\sum_i^{N_a} |\mathbf{R}_i - \mathbf{R}_{CM}|^2}{N_a} \right)^{1/2}, \tag{4.4}$$

where R_{CM} is the center of mass of the cluster and N_a is the number of atoms of the cluster. This CV gives information about how disperse the system is with regard to the center of mass. Initial tests showed that all Ag_5 and Ag_6 isomers appeared discriminated in the space of the radius of gyration and coordination number variables. In this way, C and R enable extracting information on the shape of the cluster and allow differentiating the free-energy minima found by DFT optimization, which are expected to be the centroids of each state in the free-energy landscape.

To evaluate the suitability of this set of CVs with greater precision, we performed several unbiased MD in ASE with different initial conditions, for 10000 steps with a 5 fs time-step using the Born-Oppenheimer Approximation. The electronic distribution was obtained with the LCAO-pvalence basis in a cubic cell of 16 Å with periodic boundary conditions (PBC) in all directions, using the GPAW calculator[58]. The temperature was controlled with a Berendsen thermostat at 10 K with a τ_t of 50 fs (the same setup that will be used in WT-MTD for a wider range of temperatures). Starting from the trapezoid state and bipyramidal state, we observe that the form of the basins in the space of these CVs were tilted ellipsoids in the unbiased MD (Fig. 4.4). Moreover, by performing short WT-MTD along these CVs, we noticed that there were isomers with broken bonds or that formed linear clusters, which are not of interest in the isomerization process and would require prohibitively larger computational cells (D). Therefore, there are regions of the space that are thermodynamically irrelevant. To avoid enhancing exploration toward these regions, we created a new set of CVs (CV1 and CV2) that are a rotation of C and R, over which we could easily apply a restrictive potential (equation 4.7) that we call a wall. After proving many options and ensuring that the walls do not affect the reconstructed free energy, we defined the rotated CVs as

$$CV1 = 0.99715\ C - 0.07534 \text{Å}^{-1}\ R\,, \tag{4.5}$$

$$CV2 = 0.07534\ C + 0.99715 \text{Å}^{-1}\ R\,. \tag{4.6}$$

As will be described below, we find it advantageous that the CV2 variable is an adequate CV that allows to represent the FES of Ag_6 in 1D.

4.3.1 Metadynamics-parameter determination

We used the unbiased MD trajectories to determine the optimal parameters for the WT-MTD simulation. By monitoring the CVs as a function of time, we can estimate the MTD Gaussian width, which should approximate the amplitude of the CV at each minimum (bars in Fig. 4.5). In other words, the Gaussian widths are on the same order as the variation of the CVs in the unbiased simulation. Therefore, we choose the values of σ_{CV1} and σ_{CV2} fixed to 0.3 and 0.03,

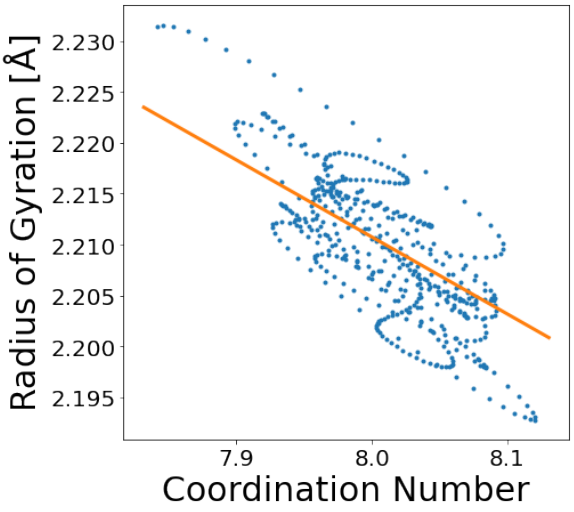

Figure 4.4: Example of the unbiased MD trajectory at 10 K starting from the trapezoidal state (dots) in the space of the collective variables coordination number and radius of gyration. The direction of the collective variable CV1 is shown as a solid orange line and CV2 is orthogonal to it.

respectively.

To choose the other WT-MTD parameters, we performed several simulations using classic MTD to have an idea of the barrier height between different states, and extracted an optimal setup. From this exploration step, we decided to fix the initial height to 0.3 eV for Ag_5 and 0.2 eV for Ag_6. The bias factor was fixed at 500, 100, and 50 for the temperatures 10, 100, and 300 K, respectively. This enabled the system to jump from the deepest minimum, but with the Gaussians decreasing fast enough to achieve convergence in the simulated steps.

Another detail of the WT-MTD setup is that the bias could make the atoms dissolve in vacuum or explore irrelevant zones of the CV space. To avoid this, we added a restraining potential (called lower or upper wall), which restrains the simulations to be lower or greater than a certain value of the CV space (a)[70,71,72]. In the case of the lower wall, it is

$$V(CV) = \begin{cases} \kappa(CV - a)^2 & \text{if } CV < a \\ 0 & \text{otherwise} \end{cases} \tag{4.7}$$

where κ is a parameter representing the strength of the restraint. For the upper wall, the $CV < a$ condition is inverted.

In Table 4.2, we show a summary of the parameters used in the simulations. It is divided in the DFT, WT-MTD, and NVT-MD simulations for Ag_5 and Ag_6.

Here, we include a note on the validity of our simulations at low temperatures. We expect only a small variation between the computed zero-temperature energy obtained via DFT op-

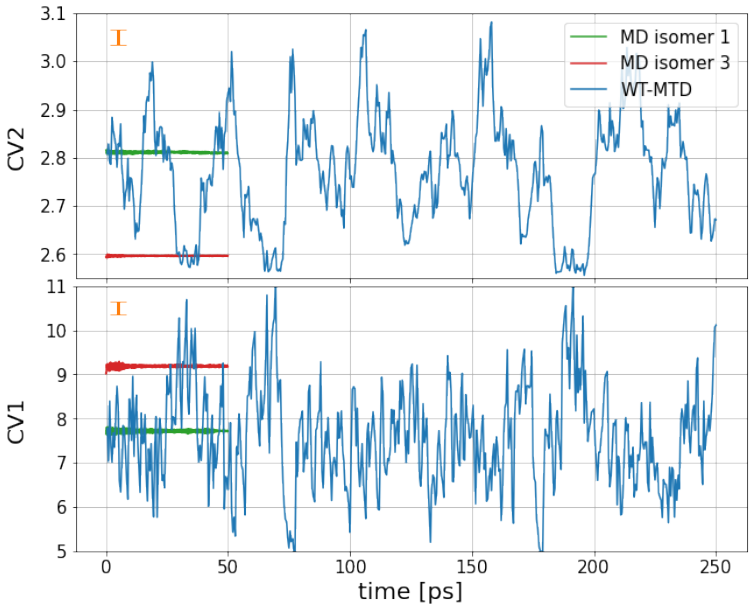

Figure 4.5: Example of the evolution of CV1 and CV2 in MD without bias and with biased WT-MTD at $T = 10K$. Red and green lines are unbiased MD simulations starting from Ag_5 states 1 and 3 from Fig. 4.1. The maximum variation range was used to set the Gaussian width σ_{CV1} and σ_{CV2} (shown as a bars). Blue lines represent the evolution of the collective variables in the WT-MTD.

timization and the 10K free energy obtained with *ab-initio* MTD. This is expected because of the underlying assumptions of fixed Boltzmann statistics in MTD and Born-Oppenheimer electron-nucleus decoupling in DFT. Therefore, we use the 10K FES values as a convergence check inside our trend study. Quantum effects that are not valid under these assumptions will not be captured in our simulations. To include quantum effects, a quantum distribution would be necessary instead of a Bolztmann's distribution[38].

4.4 Ag_5 FES from low to room temperature

Using the parameters and CVs described above, we performed WT-MTD on Ag_5 clusters for 11 independent replicas and 50000 steps, resulting in a total of 250 ps. We obtained a clear difference in the exploration of the configurations compared to the unbiased simulation. For WT-MTD, the CVs filled the metastable state smoothly and many transitions between states were observed. As a consequence, the system explored a large range of values in comparison to the maximum range covered by the simulations without bias (Fig. 4.5). This demonstrates that the free-energy landscape is being filled by the bias potential and that the system is re-crossing the relevant metastable states. Importantly, we remark that it is not enough to find

Table 4.2: Chosen parameters of NVT-MD, DFT and WT-MTD for simulations of Ag_5 and Ag_6 at 10, 100, and 300 K.

NVT-MD	Δt = 5 fs
	τ_t = 50
	T = 10 K, 100 K, 300 K
DFT	E_{xc} = PBE
	basis = LCAO-pvalence
	spin = True
WT-MTD	W = 0.3 (Ag_5) / 0.2 (Ag_6)
	CVs = CV1, CV2
	σ_{CV1} = 0.3
	σ_{CV2} = 0.03
	γ = 500 (10K) / 100 (100K) / 50(300K)
	τ = 100 steps
	$CV1$-L_{wall} at 3.(Ag_5) / 8.0 (Ag_6) κ = 10
	$CV2$-U_{wall} at 5.(Ag_5) / 3.3 (Ag_6) κ = 50

one single transition, as the free-energy reconstruction will be poor. Therefore, the simulations ran until the error (calculated using N trajectories) was in the order of tens of meV, which usually implies more than 4 transitions between minima.

We estimated the free-energy surface in the space of CV1 and CV2 as the average of the free energy for the 11 trajectories (see one example of a trajectory in Fig. D.8) for three different temperatures: 10K, 100K, and 300K (Fig. 4.6 (top)). For all temperatures, the free-energy landscape contains only two minima, although four minima are obtained from optimization. At these temperatures, states 2 and 4 (shown in Fig. 4.2), corresponding to the edge-capped square and bow-tie isomers, are just saddle points that belong to state 1 (the trapezoid isomer). Therefore, only states 1 and 3 (shown in Fig. 4.2) are representative configurations of stable isomers. By increasing the temperature in Fig. 4.6, the general form of the free energy is conserved, but both minima are more populated when the temperature is higher. This is expected as the system has more thermal energy, enabling it to escape from the local minimum and occupy other states. In Fig. 4.6 (bottom), we present the standard error calculated as the standard deviation in each grid point over the root square of the number of replicas, N. It is, at most, in the order of tens of meV, but remains lower around the lowest free-energy regions, namely, in the regions close to the minima. This suggests a good reliability of the FE reconstructions.

For low temperatures, we expect only a small variation between the computed zero-temperature energy obtained via DFT optimization and the 10K free energy obtained with *ab-initio* MTD. This is due to underlying assumptions of fixed Boltzmann statistics in MTD and Born-Oppenheimer

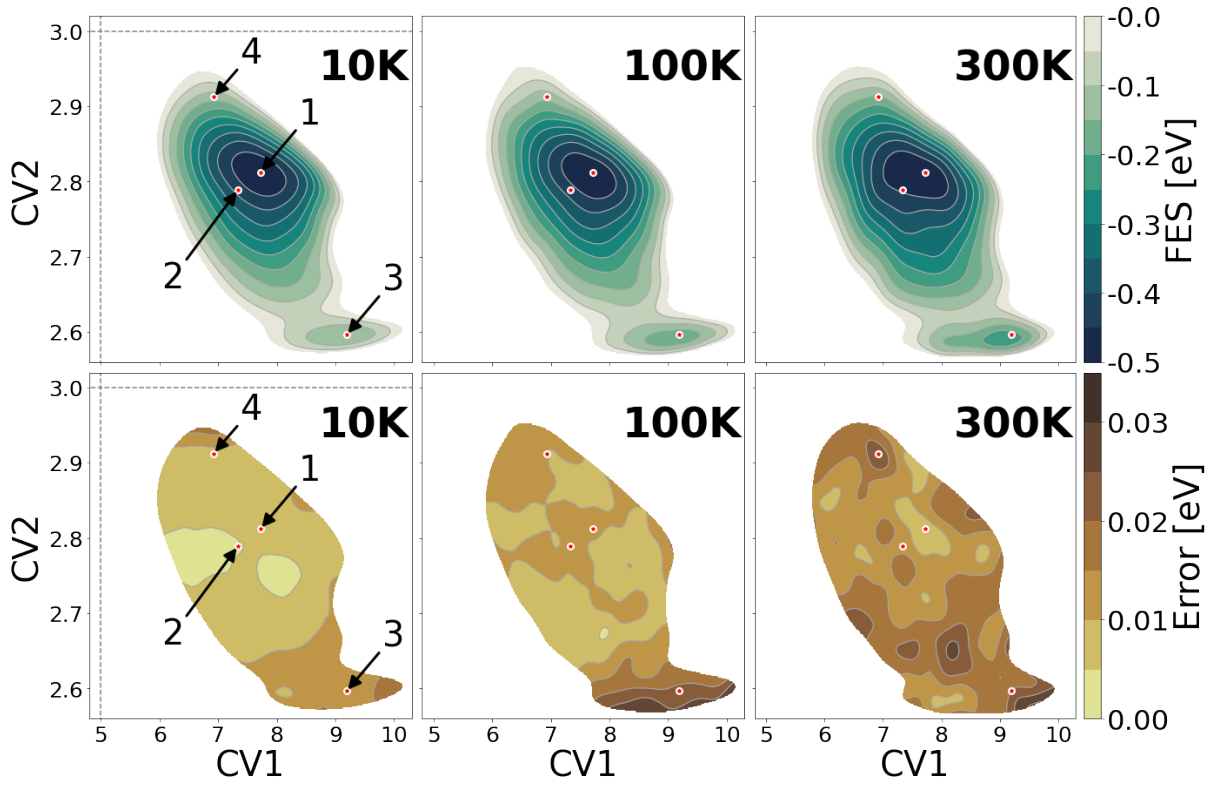

Figure 4.6: Free-energy surface of Ag_5 and error obtained in the space of the CVs CV1 and CV2 at temperatures of 10K, 100K, and 300 K. Dashed lines in 10 K are the limit of the lower (vertical) and upper (horizontal) walls that avoid an exploration towards high energy regions. Level curves are placed every 0.05 eV for the FES and every 0.005 eV for the error. The positions of isomers (Fig. 4.1) are shown as dots.

electron-nucleus decoupling in DFT. We therefore use the 10K FES values as a convergence check inside our trend study, which converge to the expected values. We note that quantum effects that are not valid under these assumptions will not be captured in our simulations. The effect of increasing the temperature is given by a decrease in the minimum activation barrier and the free-energy difference between the planar and non-planar isomers. These results are shown in Fig. 4.7, finding that, from 10K to 300K, the transition barrier decreases by approximately 0.03 eV and the free energy difference decreases by 0.09 eV, with an error of 0.02 eV at most.

A more dramatic change is captured when calculating the relative population of the basins using the Boltzmann factor. We define a basin as the region where the free-energy surface is less than the value of the minimum activation barrier (Fig. 4.7). Then, we obtained the probability of each state by integrating the Boltzmann factor over the corresponding basin, *i.e.* the

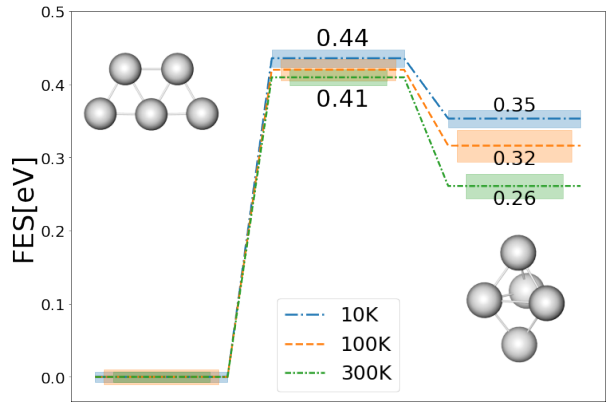

Figure 4.7: Minimum activation barrier and free-energy of the state 3 (shown at right) relative to the free-energy of state 1 (shown at left) at temperatures 10, 100 and 300 K for Ag5 cluster. Shadow colored rectangles correspond to the error.

probability of state 1 is $P_1 = \int_1 exp(-\beta F(\mathbf{s}))d\mathbf{s}$ where $\beta = 1/(k_B T)$ and $F(\mathbf{s})$ is the free-energy at $\mathbf{s}$. Interestingly, the probability associated to all the non-planar isomers is negligible for all temperature ranges (even $300K$), namely, the probability of finding a planar configuration is 100% for Ag_5.

Using statistical bootstrapping with 50 resamples, we explored how many independent simulations are required to extract an error by varying the number of samples in each resampling. This gives a notion of how the predicted result changes as a function of the number of simulated replicas. In Fig. 4.8, we show the mean value (dots) and the standard deviation (bars) of the difference in free-energy between isomers 1 and 3 of Ag_5. This result demonstrates the importance of running at least 4 replicas for obtaining a reliable free-energy difference estimate. We note that when using only one MTD simulation, the results can change significantly, even up to 0.15 eV, which is a large variation when compared with the value of this observable. This demonstrates the importance of considering several replicas for relatively short simulations in comparison with convergence criteria for one replica metadynamics that require larger simulations[73,8]. We note that the exact convergence rate will also depend on the complexity of the particular system, the simulation length, and the WT-MTD setup.

4.5 Ag_6 FES from low to room temperature

We also studied the free-energy landscape of the Ag_6 cluster, running 4 independent trajectories with 136000 steps, resulting in a total of 680 ps (see one example of a trajectory in Fig. D.9). The cluster has three stable isomers according to the optimization analysis (Table 4.1 and Fig. 4.2). In Fig. 4.9 (top), we show the FES along both CVs at the simulated

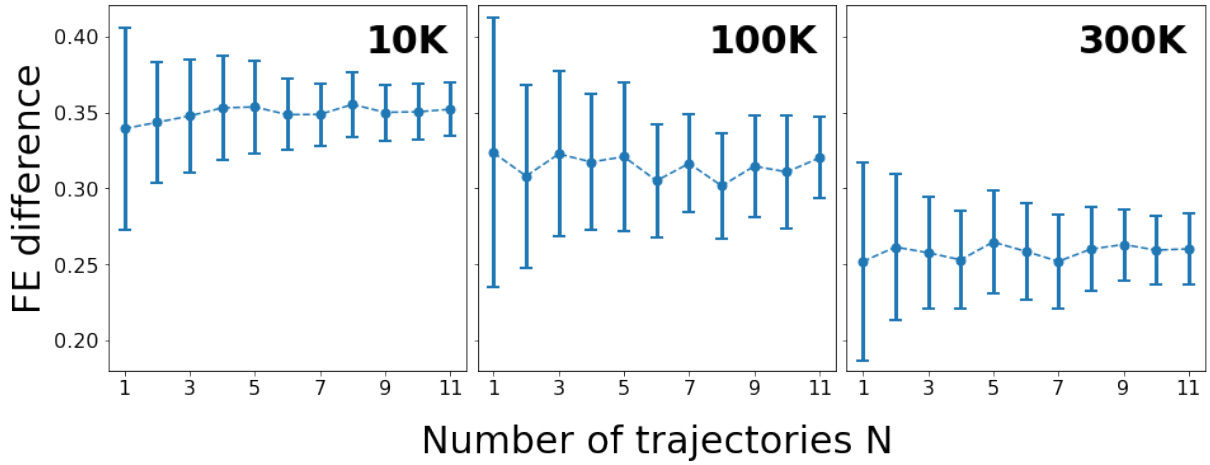

Figure 4.8: Bootstrap analysis of the difference between the Ag_5 free-energy minima, state 1 and state 3, in terms of the number of bootstrap samples. The mean (dots) and standard error (bars) are shown. As the number of samples increases, the error decreases.

temperatures. We note that only isomers 1 and 2 are stable states of the free-energy landscape. The incomplete hexagon isomer, the third Ag_6 isomer, appears as part of the basin of isomer 1. From this, it is clear that states 1 and 2 are properly separated along CV2. Therefore, integrating CV1 enables a clear representation of a free-energy profile along CV2 (*i.e.* $\exp(-\beta F(CV2)) = \int \exp(-\beta F(CV1, CV2))\, dCV1$.). The averaged profile over the 4 trajectories and a shaded region representing the standard error are shown in Fig. 4.9 (bottom). For all three cases, the standard error remains lower than 0.04 eV.

From 10 K to room temperature, the free-energy difference decreases approximately by 0.2 eV, but the barrier with respect to the global minima decreases by only 0.02 eV. In terms of probability, however, the change is drastic. At room temperature, the probability of non-planar isomer reaches 10%, which shows that the system reaches a new equilibrium where planar and non-planar isomers are competing. This is a marked difference between Ag_5 and Ag_6, and it is in accordance to an observed change in optical spectrum experiments performed by Lecoultre et al.[66] that show the absorption spectrum of Ag_n silver clusters, with n = 1-9 using sputtering technique[74]. There, experiments of the authors predict a complete domain of the isomer 1 for Ag5 (also predicted by Haslett et al. with Raman resonance spectrum[63]). Moreover, they observed an absorption expectrum that could correspond to the presence isomer 1 and 3. However, they explained the absorption peaks with a weak interaction with the deposited Argon matrix and discarded the possibility of mixture of isomers based on the zero-temperature approximation.

To gain insight into the isomerization path as a function of temperature, we have plotted

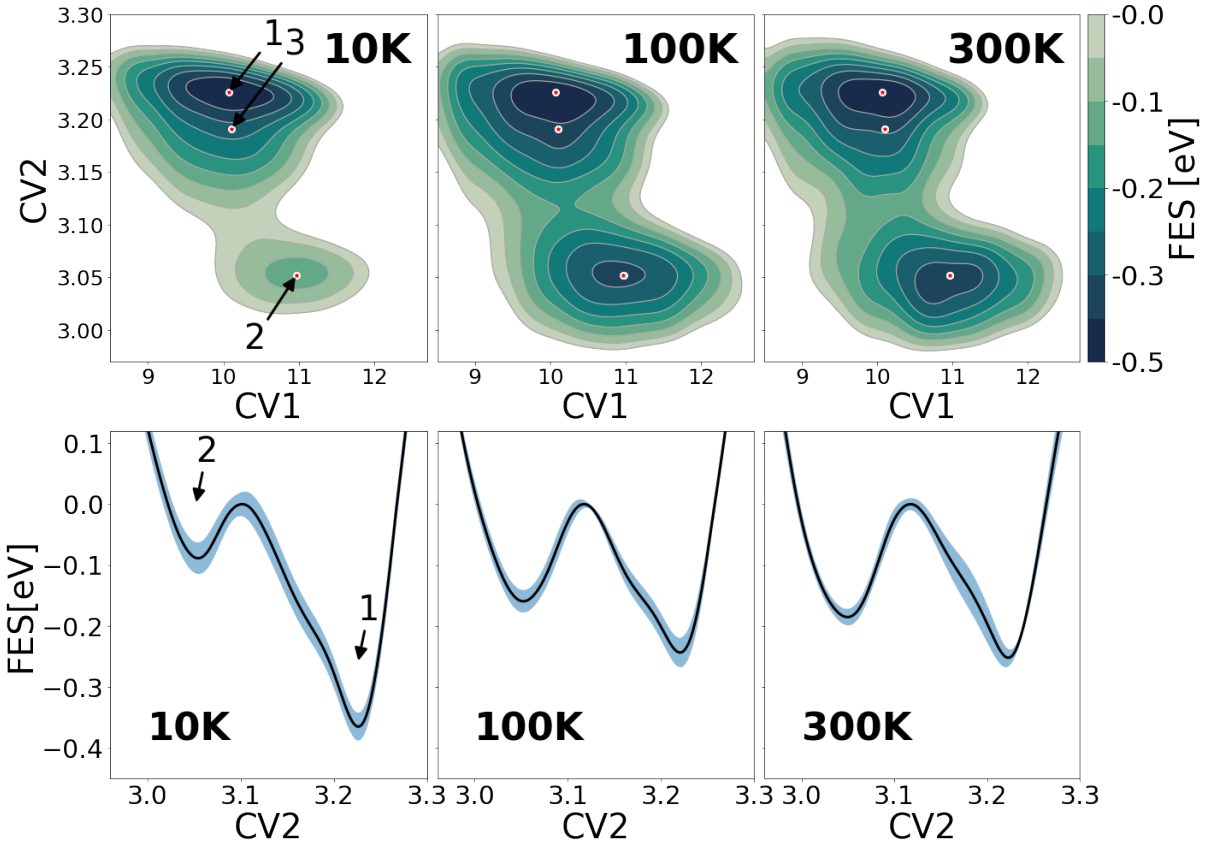

Figure 4.9: (Top) Reconstructed Free-energy surface of Ag_6 in the space of CV1 and CV2 at temperatures 10K, 100K, and 300 K. The level curves are placed each 0.05 eV. (Bottom) Free-Energy profile of Ag_6 at 10, 100, and 300 K along the collective variable CV2 with CV1 integrated out. The shaded region shows the standard error. The positions of the isomers, from Fig. 4.2, are highlighted with arrows.

the free-energy surface of Ag_5 and Ag_6 at 10, 100, and 300K, pointing out the position of the transition state[4] at T=0K (magenta stars in Appendix D, Fig. D.5 and D.5). We also extracted a few configurations close to the transition region of the reconstructed free-energy surface (blue star in Fig. D.5 and blue and orange stars in Fig. D.6). These results show that the transition path followed for the isomerization of the cluster is well represented by the T=0K simulation.

Finally, it can be noted that, at 10K, the free-energy difference is higher than expected from the ground-state DFT calculation. This can be explained by the fact that the projection of the 3N real space onto the CV space implies degenerated points: the free-energy surface corresponds to the free-energy of a set of configurations with different potential energies. This is illustrated in Appendix D, Fig. D.7. We note that degeneracies can happen when using a small

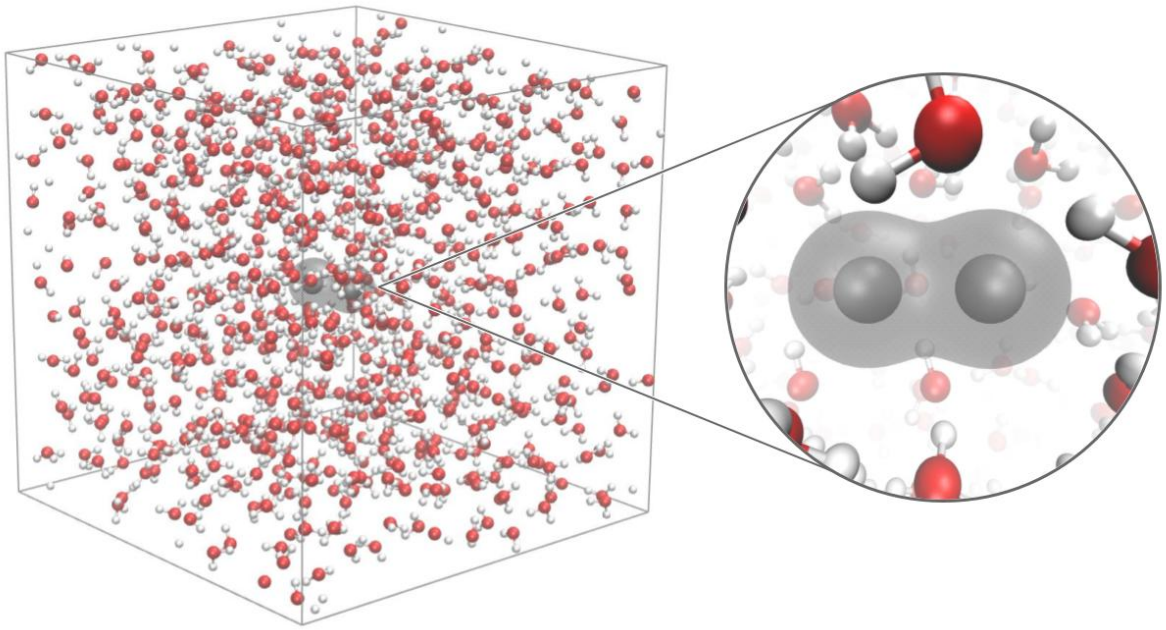

Figure 4.10: Illustration of the system simulated with QM/MM. (Left) Equilibrated periodic box, where the silver dimer is embedded. (Right) Zoomed-in dimer with an isosurface of its electronic density. Color code: dark gray = Ag, red = Oxygen, white = Hydrogen.

number of CVs to represent the entire configurational space.

4.6 Ag_2 FES including environmental effects at room temperature

We performed WT-MTD of Ag_2 embedded in an aqueous medium using QM/MM (Fig 4.10). The water-molecule interactions were modeled with a TIP3P force field[75]. In this simulation, the density of the water was 997 kg/m2 that corresponds to the liquid phase, and the hydrogen bonds lengths were fixed with RATTLE constraint[76]. The first step was to equilibrate a periodic cubic box with 27 water molecules at 300 K, starting from a crystal configuration and using a Langevin thermostat during 4000 steps, with a friction parameter equal to 0.01 and with a time step of 1 fs. Then, we replicated this box three times in each Cartesian direction to re-equilibrate this bigger box using a Berendsen thermostat, with a time step of 2 fs and a τ_t equal to 10 fs. This way, we simulated an equilibrated water environment represented by 729 water molecules in a periodic box. We used this system as SS in the QM/MM application (equation 2.34).

Then, we placed the silver dimer in the center of the water box –removing overlapped water

molecules– and defined it as the PS for the QM/MM method (equation 2.34), with a quantum cell of 20 Å and the same DFT setup used for Ag_5 and Ag_6. We approximated the non-electrostatic interaction between the PS and SS with an LJ potential. The parameters of the LJ potential were fitted to equation 2.36, considering the interaction between one water molecule and the silver dimer, varying the distance between them (Fig 4.11). Thereby, we obtained that the LJ parameters that better approximate the non-electrostatic interactions, E_{NES}, are ε equal to 0.09385 eV and σ equal to 2.77 Å.

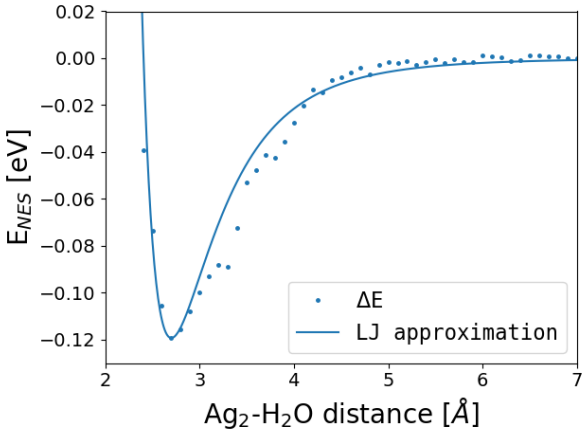

Figure 4.11: E_{NES} approximation for the silver dimer and a water molecule. The dots represent the expected interaction energies defined in equation 2.36, and the solid line is the LJ potential used in the QM/MM implementation.

We reconstructed the free-energy surface of the dimer dissociation in vacuum and embedded it in water solvent using WT-MTD. We used the distance between silver atoms as the CV (denoted by d), an initial height of 1 eV, a Gaussian width (σ_d) of 0.3 Å, a deposition rate of 50 steps, a bias factor of 50, and a simulation length of 10000 steps. We ran 4 independent replicas, as done for the LJ system, Ag_5 and Ag_6.

Figure 4.12 shows the reconstructed free-energy profiles. It is clear that the aqueous medium changes the free-energy landscape. With the water environment, the dissociated state becomes a stable state, or rather, metastable, as it is not the global minimum and there is a barrier between the bound and dissociated states, which does not exist in the vacuum case. This barrier implies that the creation of the dimer bond consumes energy. Moreover, the transition from the bonded dimer to the dissociated state has a lower free-energy barrier, which means the water destabilizes the Ag-Ag bond.

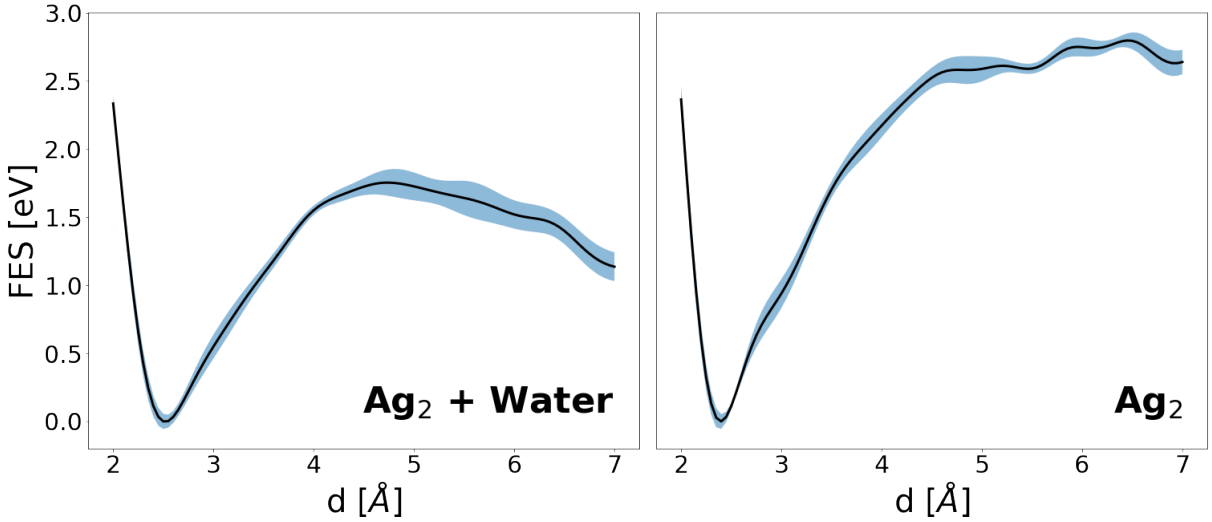

Figure 4.12: Free-energy profile of Ag_2 as function of the Ag-Ag distance at 300 K embedded in water using QM/MM (left) and in vacuum (right). Shadow region represents the standard error obtained from 4 independent replicas.

5
Conclusions

We developed a new calculator for ASE called Plumed by patching the open-source code ASE and the PLUMED plug-in, which can be used for running simulations of enhanced sampling methods. This calculator was tested with a simple system of seven LJ atoms as benchmark. This ASE-PLUMED interface was used for studying Ag_5 and Ag_6 clusters at different temperatures. We found crucial thermal effects on the Ag_6 system, which changes from a planar-dominated population at low temperatures to a state with a mixture of planar and non-planar isomers at room temperature. Because no changes in population are found in Ag_5 at the same temperature range, it follows then that Ag_6 is the smallest silver cluster with a 2D-3D isomer equilibrium at room temperature. In addition, we used QM/MM to prove that a water environment significantly changes the free-energy surface in the process of dimer bond rupture. Specifically, the basin of the bonded dimer becomes shallower in the presence of water solvent, which leads to conclude that a water environment promotes the dissociation of silver bonds. We did not study the dissociation mechanism, but it is clearly a consequence of the interaction with solvent molecules because this behavior is not observed in simulation of gas-phase (Figure 4.12 at left). Then, the dissociation mechanism could be related with the hydration of silver dimer, where the water molecules interferes in the space between silver-silver atoms.

6
Perspectives

The results of this project are an attempt to include more realistic conditions to the computational modeling of cluster conformations. In this sense, these results could be a starting point for considering more sophisticated models applied to systems of particular interest. A possible direction to follow is to include biomolecules as an environment in order to study the stability of silver clusters and its bactericide mechanisms[77,78]. These approaches include QM/MM approximations.

The study of Ag_5 and Ag_6 clusters is interesting because it has led to a discussion on the minimum cluster size for stabilizing 2D - 3D stable isomers. However, larger clusters are easier to synthesize experimentally and are used in different applications. The interface that we introduced has the potential of sampling more metastable conformations (via enhanced sampling) for larger clusters that were previously not accessible using QM methods alone.

From a computational point of view, this work opens the possibility of applying enhanced sampling methods with *ab-initio* precision in ASE for systems of interest. However, improvements to the computational performance could be further included, for example, using GPU parallelization. Moreover, these results can be used as a benchmark in the construction of classical force fields[20].

A

Appendix: Products of this thesis

In this appendix, we present the academic products of this research. The first page of the papers and the poster are attached as follows:

- (Article) **Daniel Sucerquia**, Cristian Parra, Pilar Cossio, & Olga Lopez-Acevedo. Ab initio metadynamics determination of temperature-dependent free-energy landscape in ultrasmall silver clusters. *The Journal of chemical physics*, 156(15), 2022.
- (Article) Olga Lopez-Acevedo, & **Daniel Sucerquia**. QM/MM Methods in Studies of Noble Metals: Copper, Silver, and Gold interacting with Biological and Organic Molecules. Advances in Physics: X, *submitted*, 2022.
- (Poster) **Daniel Sucerquia**, Pilar Cossio, & Olga Lopez-Acevedo. Using GPAW as MD calculator in metadynamics simulations. Event: GPAW 2021: Users and Developers Meeting.

Ab initio metadynamics determination of temperature-dependent free-energy landscape in ultrasmall silver clusters

Daniel Sucerquia,[1,2] Cristian Parra,[1] Pilar Cossio,[1,3,a)] and Olga Lopez-Acevedo[1,2,b)]

[1)]*Biophysics of Tropical Diseases, Max Planck Tandem Group, University of Antioquia UdeA, 050010 Medellin, Colombia*

[2)]*Grupo de Física Atómica y Molecular, Instituto de Física, Facultad de Ciencias Exactas y Naturales, Universidad de Antioquia UdeA; Calle 70 No. 52-21, Medellín, Colombia*

[3)]*Center for Computational Mathematics, Flatiron Institute, NY, USA.*

(Dated: 17 May 2022)

Ab initio metadynamics enables extracting free-energy landscapes having the accuracy of first principles electronic structure methods. We introduce an interface between the PLUMED code that computes free-energy landscapes and enhanced-sampling algorithms and the ASE module, which includes several *ab initio* electronic structure codes. The interface is validated with a Lennard-Jones cluster free-energy landscape calculation by averaging multiple short metadynamics trajectories. We use this interface and analysis to estimate the free-energy landscape of Ag_5 and Ag_6 clusters at 10, 100 and 300 K with the radius of gyration and coordination number as collective variables, finding at most tens of meV in error. Relative free-energy differences between the planar and non-planar isomers of both clusters decrease with temperature, in agreement with previously proposed stabilization of non-planar isomers. Interestingly, we find that Ag_6 is the smallest silver cluster where entropic effects at room temperature boost the non planar isomer probability to a competing state. The new ASE-PLUMED interface enables simulating nanosystem electronic properties at more realistic temperature-dependent conditions.

[a)]Electronic mail: pcossio@flatironinstitute.org

[b)]Electronic mail: olga.lopeza@udea.edu.co

ARTICLE TEMPLATE

QM/MM Methods in Studies of Noble Metals: Copper, Silver, and Gold interacting with Biological and Organic Molecules

O. Lopez-Acevedo[a], D. Sucerquia[a]

[a] Biophysics of Tropical Diseases, Max Planck Tandem Group, University of Antioquia UdeA, 050010 Medellin, Colombia

ARTICLE HISTORY
Compiled March 14, 2022

ABSTRACT
A QM/MM method is an atomistic simulation algorithm that allows researchers to describe different regions of a system with different physical laws. Here, we review this hybrid method's applications to the study of copper, silver, and gold atoms and clusters interacting with biological and organic molecules. In particular, we highlight efforts to characterize the relaxation process in a copper(I) phenanthroline complex; details of Cu's secretory path; the atomic structure of Ag-homopolymers of cytosine and guanine; DNA-stabilized silver clusters; effects related to temperature and solvent on thiolate-protected gold clusters' optical properties; and the effect of a medium-like noble gas on a cluster's optical spectrum. The results of these efforts demonstrate how QM/MM methods are applied succesfully to a wide range of processes that include the study of excited state evolution, charge transport, light absorption and emission, and determining an atomic structure in absence of crystal-determined structure. We expect QM/MM methods will continue supporting the exploration of novel hybrid organo-metallic materials and their safe use in the environment, while also providing guidance on mechanisms to deal with diseases associated with a failure in cells' proper behavior.

KEYWORDS
QM/MM; metal-organics; Copper-mediated; DNA-stabilized clusters; thiolate-protected gold clusters

1. Introduction

Metals exist in many fundamental biological processes and form hybrid complexes with organic matter. Copper, for example, is essential to copper-mediated enzymes that regulate oxygen transport and communication between neurons [1], and iron is present in hemoglobin and oxygen transport processes [2]. To date, nanoscience has offered some exploration of hybrid metalo-organic materials, such as DNA-stabilized silver clusters [3–5] and thiolate-protected gold clusters [6, 7] with potential applications as biosensors, in bioimaging and medicine[8, 9]. Yet within these systems, many properties and possibilities remain unexplored. Other knowledge we might gain about these metals in hybrid form include questions on their stability in solution, which are important questions in potentiating their use in technological applications.

To better understand and push beyond the body of research amassed thus far,

Email: olga.lopeza@udea.edu.co

Using GPAW as MD Calculator in Metadynamics Simulations

Daniel Sucerquia[1] , Pilar Cossio[2,3] and Olga Lopez-Acevedo[1,2]
[1] Grupo de Física Atómica y Molecular, Universidad de Antioquia UdeA, Medellin, Colombia.
[2] Biophysics of Tropical Diseases Max Planck Tandem Group, University of Antioquia, Medellín, Colombia.
[3] Center for Computational Mathematics, Flatiron Institute, NY, USA.

UNIVERSIDAD DE ANTIOQUIA 1803

Abstract

Considering that entropic effects cannot be addressed with groundstate DFT calculations and that requires an estimation of the free energy landscape of the systems, we developed an interface to PLUMED [1] as a new calculator in ASE for carrying out enhanced sampling methods like Metadynamics [2] simulations which works together with GPAW as ab-initio calculator of the unbiased part. This calculator contains PLUMED as a plug-in for the computation of collective variables, bias forces, bias energy, and other practical tools. Here is presented an example using metadynamics with GPAW in which we obtained the free energy landscape of Ag5 cluster in terms of the collective variables radius of gyration and coordination number.

Plumed

PLUMED is an open-source, community-developed library that provides a wide range of different methods, which include:

- Enhanced-sampling algorithms
- Free-energy methods
- Tools to analyze data produced by molecular dynamics (MD) simulations

Metadynamics

Metadynamics [3] is an enhanced sampling algorithm in which the normal evolution of the system is biased by a history-dependent potential constructed as a sum of Gaussians centered along the trajectory followed by a suitably chosen set of collective variables, s:

$$V_G(s,t) = \omega \sum_{i=\tau_G,2\tau_G\ldots}^{i<t} e^{-\frac{(s-s(i))^2}{2\delta s^2}}$$

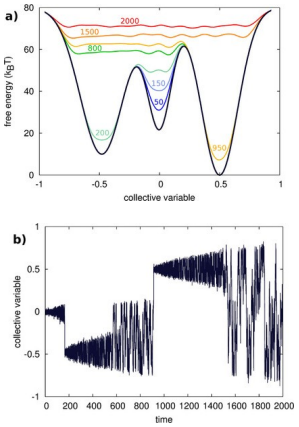

Image from [4]

And it is demonstrated that [2]:

$$\lim_{t\to\infty} V_G(s,t) = -F(s) + C$$

Plumed Calculator

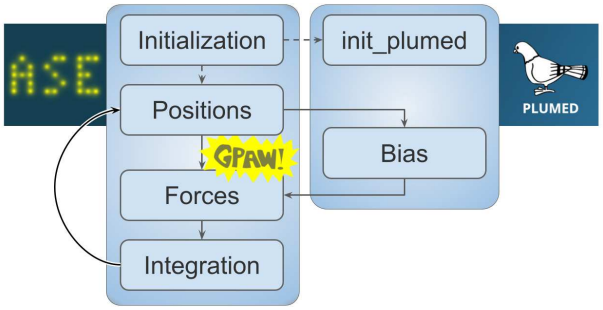

The new calculator is initialized from ASE and each time step it can compute:

- A large set of collective variables
- Bias potential energy
- Bias Forces

Ag_5 Isomers

We used this new calculator for studying the free energy landscape of Ag_5 at 10K of temperature using metadynamics in the collective variables radius of gyration and coodination number:

$$R = \frac{\sum_i^n m_i |r_i - r_{COM}|^2}{\sum_i^n m_i}$$

$$C = \sum_{i\neq j} \frac{1-(r_{ij}/r_0)^n}{1-(r_{ij}/r_0)^m}$$

We solve the unbiased forces with GPAW using LCAO and PBE.

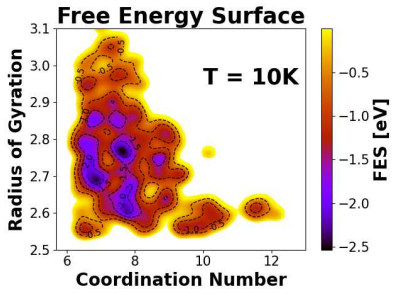

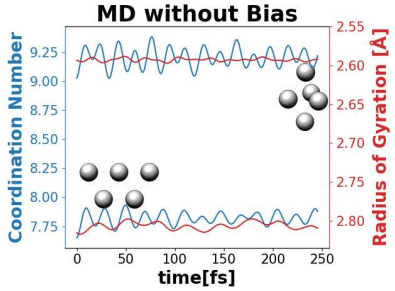

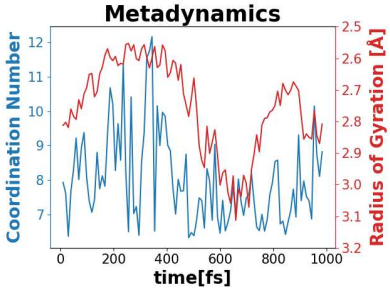

Conclusions

We have created an interface to PLUMED that can work together with GPAW for carrying out enhanced sampling methods like Metadynamics, which we used for showing a possible aplication where we study the conformational space of Ag5 clusters. Now all users of GPAW can implement the methods that plumed contains.

References

[1] Massimiliano Bonomi, Giovanni Bussi, Carlo Camilloni, Gareth A Tribello, Pavel Banáš, Alessandro Barducci, Mattia Bernetti, Peter G Bolhuis, Sandro Bottaro, Davide Branduardi, et al. Promoting transparency and reproducibility in enhanced molecular simulations. *Nature methods*, 16(8):670–673, 2019.

[2] Giovanni Bussi, Alessandro Laio, and Michele Parrinello. Equilibrium free energies from nonequilibrium metadynamics. *Physical review letters*, 96(9):090601, 2006.

[3] Alessandro Laio and Michele Parrinello. Escaping free-energy minima. *Proceedings of the National Academy of Sciences*, 99(20):12562–12566, 2002.

[4] Fabio Pietrucci. Strategies for the exploration of free energy landscapes: Unity in diversity and challenges ahead. *Reviews in Physics*, 2:32–45, 2017.

B
Appendix: Plumed calculator

```
from ase.calculators.calculator import Calculator, all_changes
from ase.io.trajectory import Trajectory
from ase.parallel import broadcast
from ase.parallel import world
import numpy as np
from os.path import exists
from ase.units import fs, mol, kJ, nm


def restart_from_trajectory(prev_traj, *args, prev_steps=None, atoms=None,
                            **kwargs):
    """This function helps the user to restart a plumed simulation
    from a trajectory file.

    Parameters
    ----------
    prev_traj : Trajectory object
        previous simulated trajectory

    prev_steps : int. Default steps in prev_traj.
```

```
        number of previous steps

    others :
       Same parameters of :mod:‘~ase.calculators.plumed‘ calculator

    Returns
    -------
    Plumed calculator


    .. note:: prev_steps is crucial when trajectory does not contain
        all the previous steps.
    """
    atoms.calc = Plumed(*args, atoms=atoms, restart=True, **kwargs)

    with Trajectory(prev_traj) as traj:
        if prev_steps is None:
            atoms.calc.istep = len(traj) - 1
        else:
            atoms.calc.istep = prev_steps
        atoms.set_positions(traj[-1].get_positions())
        atoms.set_momenta(traj[-1].get_momenta())
    return atoms.calc


class Plumed(Calculator):
    implemented_properties = ['energy', 'forces']

    def __init__(self, calc, input, timestep, atoms=None, kT=1., log='',
                 restart=False, use_charge=False, update_charge=False):
        """
        Plumed calculator is used for simulations of enhanced sampling methods
        with the open-source code PLUMED (plumed.org).

        [1] The PLUMED consortium, Nat. Methods 16, 670 (2019)
        [2] Tribello, Bonomi, Branduardi, Camilloni, and Bussi,
        Comput. Phys. Commun. 185, 604 (2014)
```

```
Parameters
----------
calc: Calculator object
    It  computes the unbiased forces

input: List of strings
    It contains the setup of plumed actions

timestep: float
    Time step of the simulated dynamics

atoms: Atoms
    Atoms object to be attached

kT: float. Default 1.
    Value of the thermal energy in eV units. It is important for
    some methods of plumed like Well-Tempered Metadynamics.

log: string
    Log file of the plumed calculations

restart: boolean. Default False
    True if the simulation is restarted.

use_charge: boolean. Default False
    True if you use some collective variable which needs charges. If
    use_charges is True and update_charge is False, you have to define
    initial charges and then this charge will be used during all
    simulation.

update_charge: boolean. Default False
    True if you want the charges to be updated each time step. This
    will fail in case that calc does not have 'charges' in its
    properties.


.. note:: For this case, the calculator is defined strictly with the
    object atoms inside. This is necessary for initializing the
```

```
    Plumed object. For conserving ASE convention, it can be initialized
    as atoms.calc = (..., atoms=atoms, ...)


.. note:: In order to guarantee a proper restart, the user has to fix
    momenta, positions and Plumed.istep, where the positions and
    momenta corresponds to the last configuration in the previous
    simulation, while Plumed.istep is the number of timesteps
    performed previously. This can be done using
    ase.calculators.plumed.restart_from_trajectory.
"""

from plumed import Plumed as pl

if atoms is None:
    raise TypeError('plumed calculator has to be defined with the \
                     object atoms inside.')

self.istep = 0
Calculator.__init__(self, atoms=atoms)

self.input = input
self.calc = calc
self.use_charge = use_charge
self.update_charge = update_charge

if world.rank == 0:
    natoms = len(atoms.get_positions())
    self.plumed = pl()

    ''' Units setup
    warning: inputs and outputs of plumed will still be in
    plumed units.

    The change of Plumed units to ASE units is:
    kjoule/mol to eV
    nm to Angstrom
    ps to ASE time units
```

```
        ASE and plumed - charge unit is in e units
        ASE and plumed - mass unit is in a.m.u units '''

        ps = 1000 * fs
        self.plumed.cmd("setMDEnergyUnits", mol/kJ)
        self.plumed.cmd("setMDLengthUnits", 1/nm)
        self.plumed.cmd("setMDTimeUnits", 1/ps)
        self.plumed.cmd("setMDChargeUnits", 1.)
        self.plumed.cmd("setMDMassUnits", 1.)

        self.plumed.cmd("setNatoms", natoms)
        self.plumed.cmd("setMDEngine", "ASE")
        self.plumed.cmd("setLogFile", log)
        self.plumed.cmd("setTimestep", float(timestep))
        self.plumed.cmd("setRestart", restart)
        self.plumed.cmd("setKbT", float(kT))
        self.plumed.cmd("init")
        for line in input:
            self.plumed.cmd("readInputLine", line)
    self.atoms = atoms

def _get_name(self):
    return f'{self.calc.name}+Plumed'

def calculate(self, atoms=None, properties=['energy', 'forces'],
              system_changes=all_changes):
    Calculator.calculate(self, atoms, properties, system_changes)

    comp = self.compute_energy_and_forces(self.atoms.get_positions(),
                                          self.istep)
    energy, forces = comp
    self.istep += 1
    self.results['energy'], self. results['forces'] = energy, forces

def compute_energy_and_forces(self, pos, istep):
    unbiased_energy = self.calc.get_potential_energy(self.atoms)
    unbiased_forces = self.calc.get_forces(self.atoms)
```

```
    if world.rank == 0:
        ener_forc = self.compute_bias(pos, istep, unbiased_energy)
    else:
        ener_forc = None
    energy_bias, forces_bias = broadcast(ener_forc)
    energy = unbiased_energy + energy_bias
    forces = unbiased_forces + forces_bias
    return energy, forces

def compute_bias(self, pos, istep, unbiased_energy):
    self.plumed.cmd("setStep", istep)

    if self.use_charge:
        if 'charges' in self.calc.implemented_properties and \
                                        self.update_charge:
            charges = self.calc.get_charges(atoms=self.atoms.copy())

        elif self.atoms.has('initial_charges') and not self.update_charge:
            charges = self.atoms.get_initial_charges()

        else:
            assert not self.update_charge, "Charges cannot be updated"
            assert self.update_charge, "Not initial charges in Atoms"

        self.plumed.cmd("setCharges", charges)

    # Box for functions with PBC in plumed
    if self.atoms.cell:
        cell = np.asarray(self.atoms.get_cell())
        self.plumed.cmd("setBox", cell)

    self.plumed.cmd("setPositions", pos)
    self.plumed.cmd("setEnergy", unbiased_energy)
    self.plumed.cmd("setMasses", self.atoms.get_masses())
    forces_bias = np.zeros((self.atoms.get_positions()).shape)
    self.plumed.cmd("setForces", forces_bias)
    virial = np.zeros((3, 3))
    self.plumed.cmd("setVirial", virial)
```

```
        self.plumed.cmd("prepareCalc")
        self.plumed.cmd("performCalc")
        energy_bias = np.zeros((1,))
        self.plumed.cmd("getBias", energy_bias)
        return [energy_bias, forces_bias]

    def write_plumed_files(self, images):
        """ This function computes what is required in
        plumed input for some trajectory.

        The outputs are saved in the typical files of
        plumed such as COLVAR, HILLS """
        for i, image in enumerate(images):
            pos = image.get_positions()
            self.compute_energy_and_forces(pos, i)
        return self.read_plumed_files()

    def read_plumed_files(self, file_name=None):
        read_files = {}
        if file_name is not None:
            read_files[file_name] = np.loadtxt(file_name, unpack=True)
        else:
            for line in self.input:
                if line.find('FILE') != -1:
                    ini = line.find('FILE')
                    end = line.find(' ', ini)
                    if end == -1:
                        file_name = line[ini+5:]
                    else:
                        file_name = line[ini+5:end]
                    read_files[file_name] = np.loadtxt(file_name, unpack=True)

            if len(read_files) == 0:
                if exists('COLVAR'):
                    read_files['COLVAR'] = np.loadtxt('COLVAR', unpack=True)
                if exists('HILLS'):
                    read_files['HILLS'] = np.loadtxt('HILLS', unpack=True)
        assert not len(read_files) == 0, "There are not files for reading"
```

```
    return read_files

def __enter__(self):
    return self

def __exit__(self, *args):
    self.plumed.finalize()
```

C

Appendix: Tests added to ASE source

```
from ase import Atoms
from ase.calculators.emt import EMT
from ase.calculators.idealgas import IdealGas
from ase.md.verlet import VelocityVerlet
from ase.calculators.lj import LennardJones
import numpy as np
from ase.io.trajectory import Trajectory
from pytest import approx
import pytest
from ase.calculators.plumed import restart_from_trajectory


@pytest.mark.calculator_lite
@pytest.mark.calculator('plumed')
def test_CVs(factory):
    """ This test calls plumed-ASE calculator for computing some CVs.
    Moreover, it computes those CVs directly from atoms.positions and
    compares them"""
    # plumed setting
    set_plumed = ["c1: COM ATOMS=1,2",
```

```
                "c2: CENTER ATOMS=1,2",
                "l: DISTANCE ATOMS=c1,c2",
                "d: DISTANCE ATOMS=1,2",
                "c: COORDINATION GROUPA=1 GROUPB=2 R_0=100 MM=0 NN=10",
                "FLUSH STRIDE=1",
                "PRINT ARG=d,c,l STRIDE=10 FILE=COLVAR_test1"]

# execution
atoms = Atoms('CO', positions=[[0, 0, 0], [0, 0, 5]])  # CO molecule
_, colvar = run(factory, [set_plumed, atoms, 5], calc=EMT(), steps=101)

# this compares the time calculated by ASE and plumed
timeASE = np.arange(0., 501., 50)
timePlumed = colvar['COLVAR_test1'][0]
assert timeASE == approx(timePlumed), "Error in time registered by plumed"

# This compares the distance of atoms calculated by ASE and plumed
distASE = np.array([5., 51.338332, 141.252854, 231.167376, 321.081899,
                    410.996421, 500.910943, 590.825465, 680.739987,
                    770.654509, 860.569031])
distPlumed = colvar['COLVAR_test1'][1]
assert distPlumed == approx(distASE), "Error in distance "

# this compares the coordination number calculated by ASE and plumed
CASE = np.array([1.0000e+00, 9.9873e-01, 3.0655e-02, 2.2900e-04, 9.0000e-06,
                 1.0000e-06, 0.0000e+00, 0.0000e+00, 0.0000e+00, 0.0000e+00,
                 0.0000e+00])
CPlumed = colvar['COLVAR_test1'][2]
assert CASE == approx(CPlumed, abs=1E-5), "Error in coordination number"

# this compares the distance between center of mass and geometrical center
# calculated by ASE and plumed
centersASE = np.array([0.355944, 3.654717, 10.05563, 16.456542, 22.857455,
                       29.258367, 35.65928, 42.060192, 48.461104, 54.862017,
                       61.262929])

centersPlumed = colvar['COLVAR_test1'][3]
assert centersASE == approx(centersPlumed)
```

```
@pytest.mark.calculator_lite
@pytest.mark.calculator('plumed')
def test_metadyn(factory):
    """This test computes a Metadynamics calculation,
    This result is compared with the same calulation made externally"""
    params = setups()
    atoms, _ = run(factory, params, steps=58)

    position1 = -0.0491871
    position2 = 6.73693
    forceWithBias = 0.28807

    assert (atoms.get_positions()[0][0] == approx(position1, abs=0.01) and
            atoms.get_positions()[1][0] == approx(position2, abs=0.01)),
            "Error in the metadynamics simulation"
    assert atoms.get_forces()[0][0] == approx(forceWithBias, abs=0.01),
           "Error in the computation of Bias-forces"


@pytest.mark.calculator_lite
@pytest.mark.calculator('plumed')
def test_restart(factory):
    ins = setups()
    # first steps
    _, res = run(factory, ins, name='restart')

    # rest of steps with restart
    input, atoms1, timestep = setups()
    with restart_from_trajectory('test-restart.traj',
                                 calc=LennardJones(epsilon=10, sigma=6),
                                 input=input,
                                 timestep=timestep,
                                 atoms=atoms1) as atoms1.calc:
        with VelocityVerlet(atoms1, timestep) as dyn:
            dyn.run(30)
```

```
    # Values computed externally
    position1 = -0.0491871
    position2 = 6.73693
    forceWithBias = 0.28807

    assert atoms1.get_forces()[0][0] == approx(forceWithBias, abs=0.01),
                    "Error in restart for the computation of Bias-forces"

    assert (atoms1.get_positions()[0][0] == approx(position1, abs=0.01) and
            atoms1.get_positions()[1][0] == approx(position2, abs=0.01)),
                    "Error in the restart of metadynamics simulation"


@pytest.mark.calculator_lite
@pytest.mark.calculator('plumed')
def test_postpro(factory):
    # Metadynamics simulation
    params = setups('direct')
    _, direct = run(factory, params, name='direct', steps=58)

    params = setups('postpro')
    # Postpro resconstruction
    with factory.calc(calc=IdealGas(),
                      input=params[0],
                      atoms=params[1],
                      timestep=params[2]) as calc:
        with Trajectory('test-direct.traj') as traj:
            postpr = calc.write_plumed_files(traj)['HILLS_postpro']

    assert postpr == approx(direct['HILLS_direct'])


def run(factory, inputs, name='',
        calc=LennardJones(epsilon=10, sigma=6),
        traj=None, steps=29):
    input, atoms, timestep = inputs
    with factory.calc(calc=calc,
                      input=input,
```

```
                    timestep=timestep,
                    atoms=atoms) as atoms.calc:
        with VelocityVerlet(atoms, timestep,
                            trajectory='test-{}.traj'.format(name)) as dyn:
            dyn.run(steps)
        res = atoms.calc.read_plumed_files()
    return atoms, res


def setups(name=''):
    set_plumed = ["d: DISTANCE ATOMS=1,2",
                  "FLUSH STRIDE=1",
                  "METAD ARG=d SIGMA=0.5 HEIGHT=2 PACE=20 " +
                  "FILE=HILLS_{}".format(name)]
    atoms = Atoms('CO', positions=[[0, 0, 0], [6.7, 0, 0]])
    timestep = 0.05
    return set_plumed, atoms, timestep
```

D

Appendix: Silver configurations

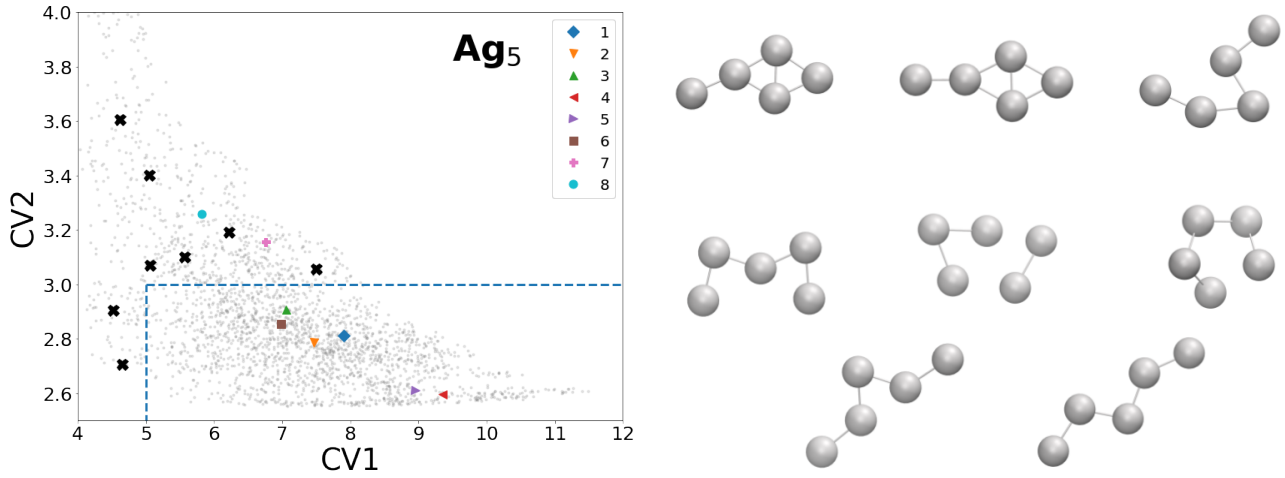

Figure D.1: (a) Trajectory of metadynamics simulation without walls (gray points) for Ag_5 in the space of the collective variables CV1 and CV2 defined in equations 8 and 9 of the main text. Colored markers show the location of the isomers presented in Figure D.2. Black Xs correspond to example configurations presented on the panel (b), which are excluded by the walls (dashed lines). Lines between atoms in configurations represent distances lower than 3 Å.

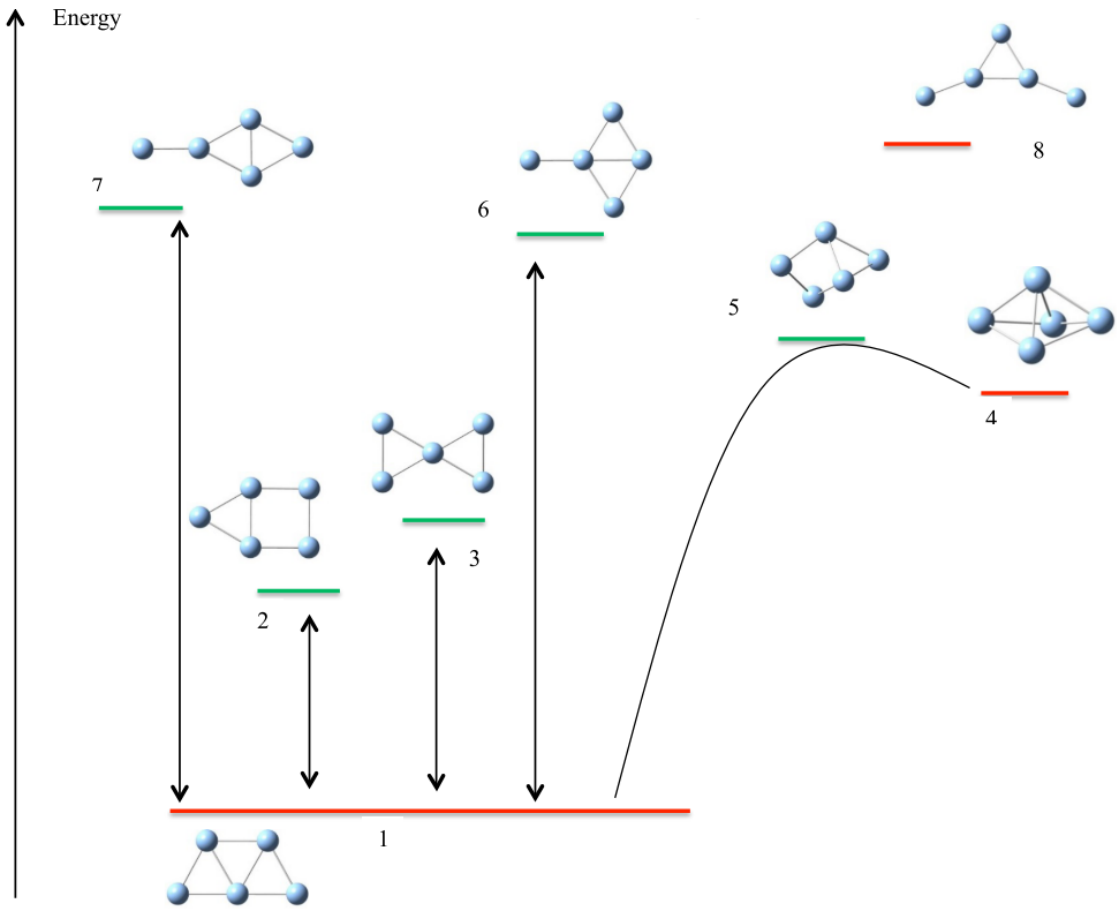

Figure D.2: Ag_5 isomers optimized with N12/jun-cc-pVTZ-PP. The order of the isomers corresponds to the order of the potential energies. Green lines are saddle points, red lines represent local minima. Reprinted with permission from Duanmu and Truhlar[4]. Copyright 2015 American Chemical Society.

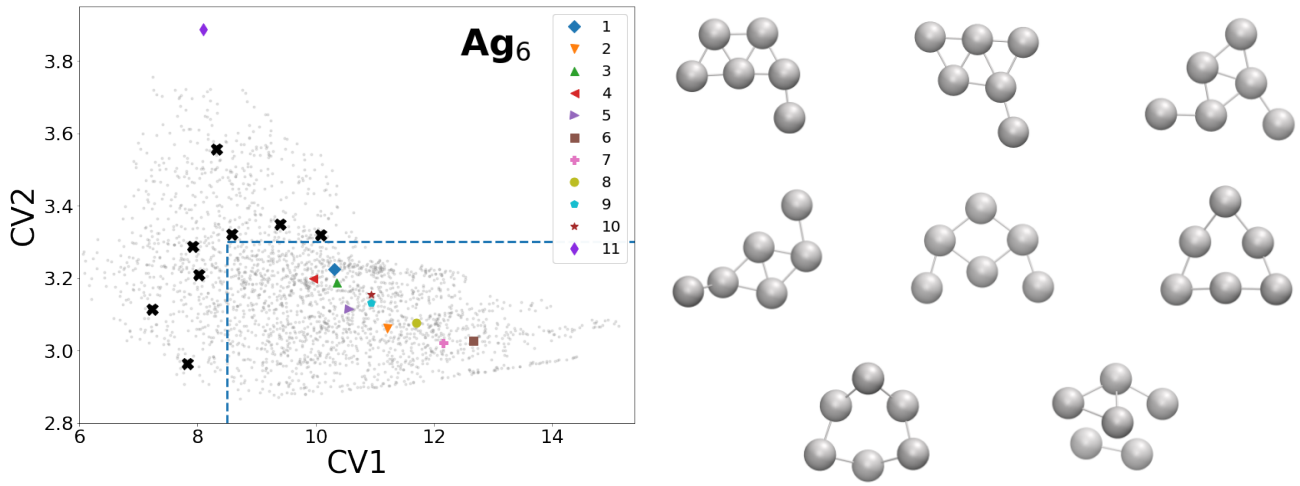

Figure D.3: (a) Trajectory of metadynamics simulation without walls (gray points) for Ag_6 in the space of the collective variables CV1 and CV2 defined in equation 8 and 9 of the main text. Colored markers show the location of the isomers presented in Figure D.4. Black Xs correspond to example configurations presented on the panel (b), which are excluded by the walls (dashed lines). Lines between atoms in configurations represent distances lower than 3 Å.

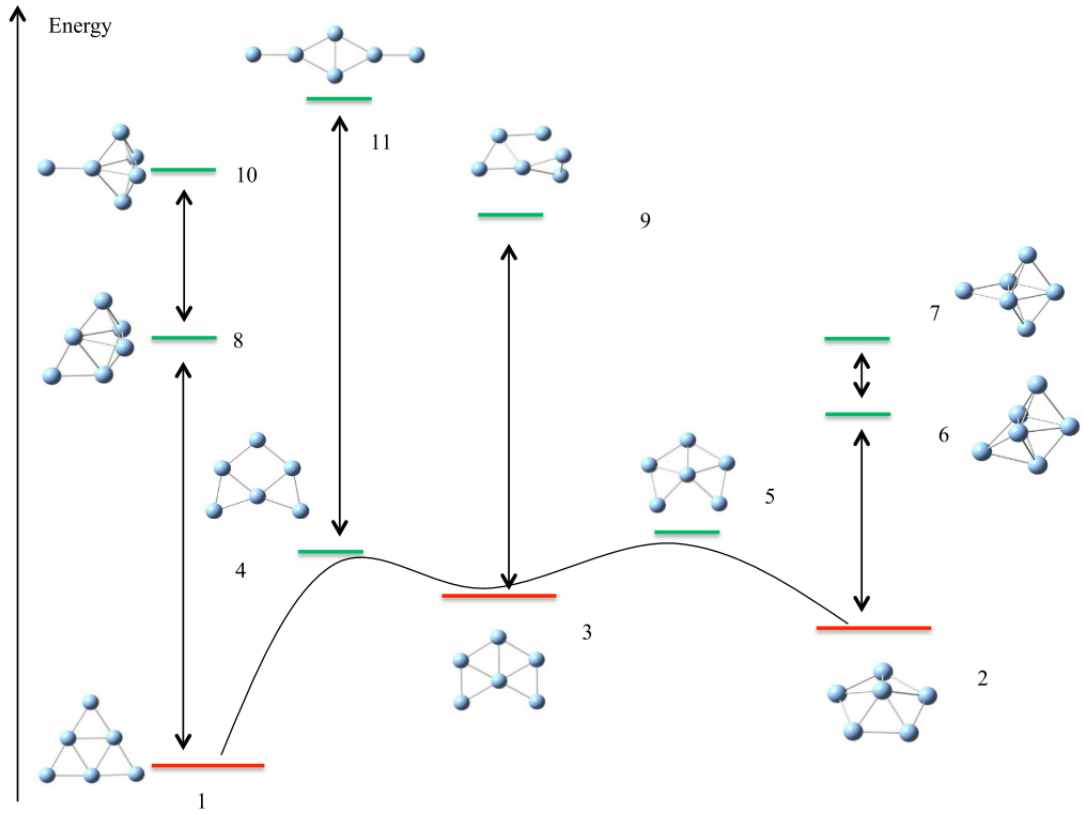

Figure D.4: Ag_6 isomers optimized with N12/jun-cc-pVTZ-PP. The order of the isomers corresponds to the order of the energies. Green lines are saddle points, red lines represent local minima. Reprinted with permission from Duanmu and Truhlar[4]. Copyright 2015 American Chemical Society.

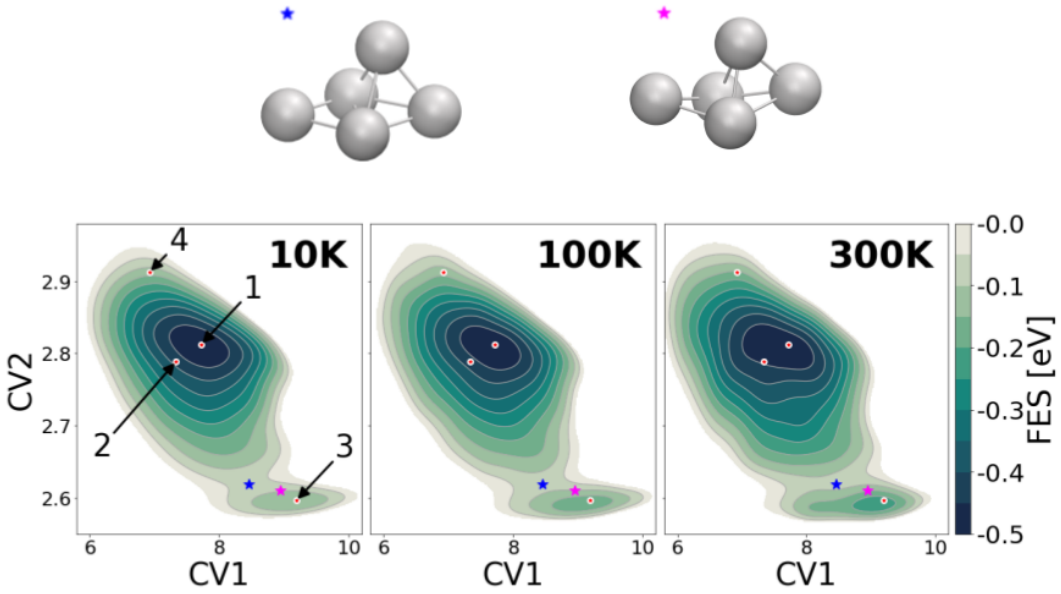

Figure D.5: Ag_5 approximate transition points over the obtained free-energy surface in the space of collective variables CV1 and CV2. The magenta star corresponds to the transition configuration obtained by Duanmu and Truhlar[4] with N12/jun-cc-pVTZ-PP (Figure D.2). The blue star is an example of a configuration obtained from the WT-MTD simulations that approximates to the transition point.

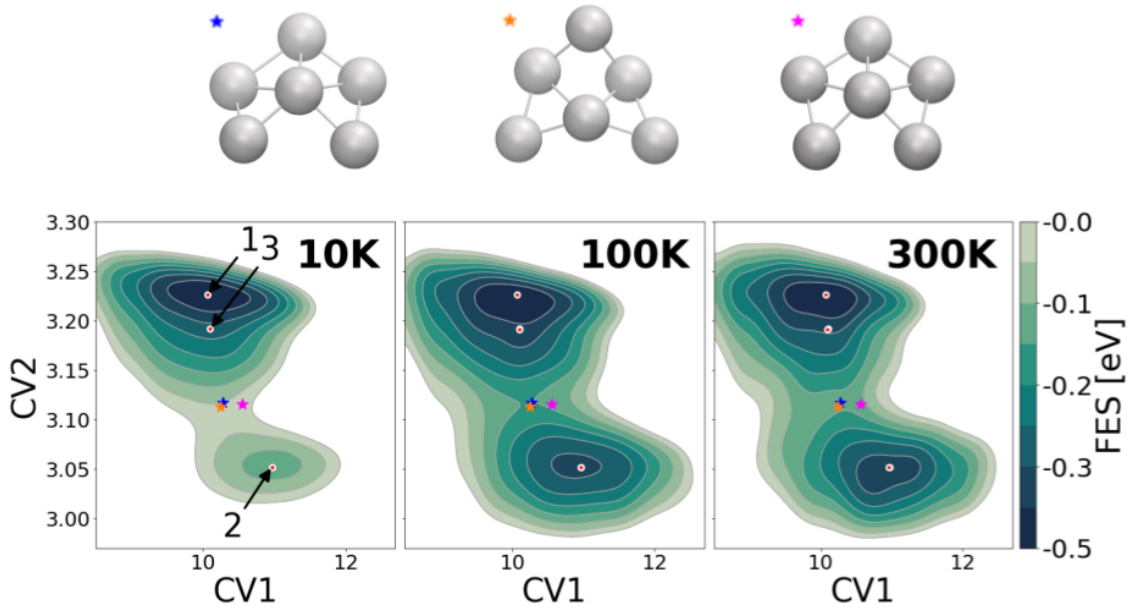

Figure D.6: Ag_6 approximate transition points over the obtained free-energy surface in the space of collective variables CV1 and CV2. The magenta star corresponds to the transition configuration obtained by Duanmu and Truhlar[4] with N12/jun-cc-pVTZ-PP (Figure D.4). The blue and orange stars are example configurations obtained from the WT-MTD simulations that approximate to the transition point.

D.1 Degenerated configurations in CV space

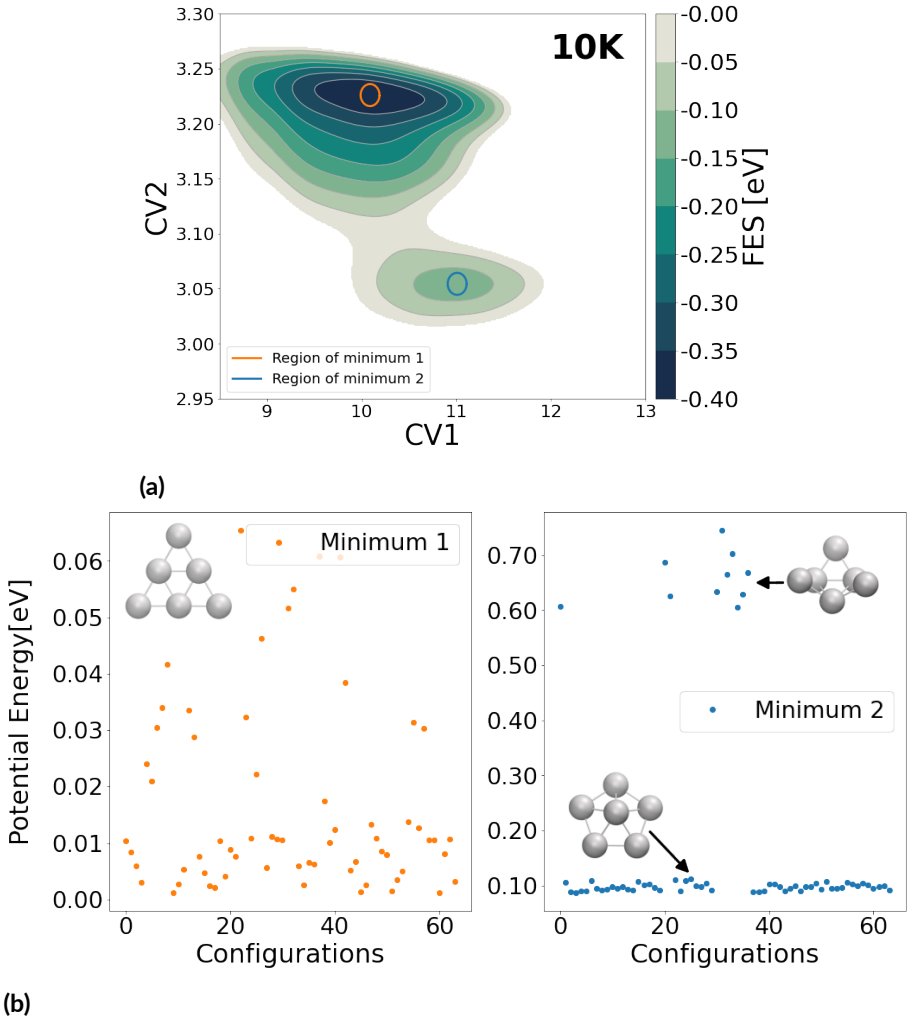

Figure D.7: Potential energy of a set of configurations close to the minima in the Ag6 free-energy surface at 10K. (a) Regions in CV space selected to extract the random configurations close to the minima corresponding to isomer 1 and isomer 2 shown in Figure 2 of the Main Text. b) Potential energy of the set of configurations (orange and blue are configurations near to minimum 1 and 2, respectively). Examples of selected configurations are shown as inset. Lines between atoms in configurations represent distances lower than 3 Å.

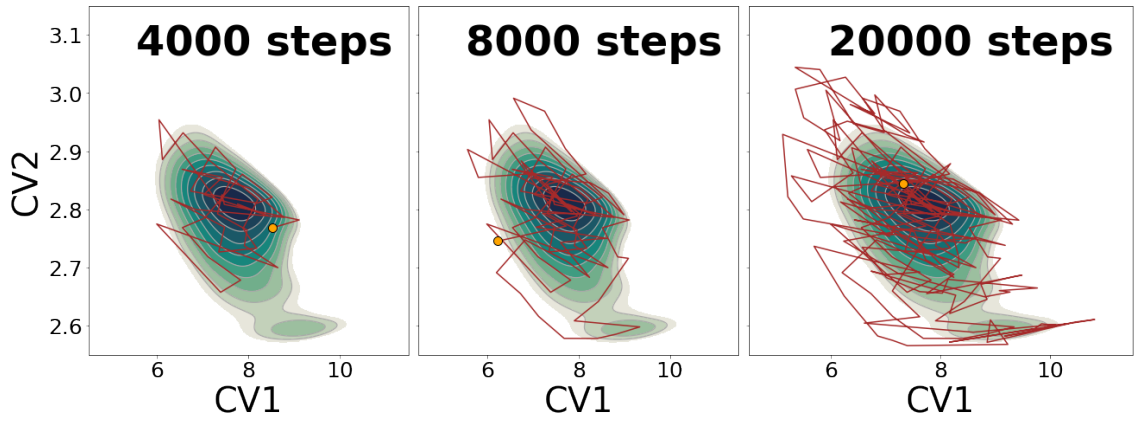

Figure D.8: First 4000, 8000 and 20000 steps of one Ag_5 WT-MTD trajectory (brown line) in CV1-CV2 space over the free energy surface at 10 K presented in Fig. 4.6. The points in the trajectory were taken each 100 steps. The Orange dot represents the position of the last step.

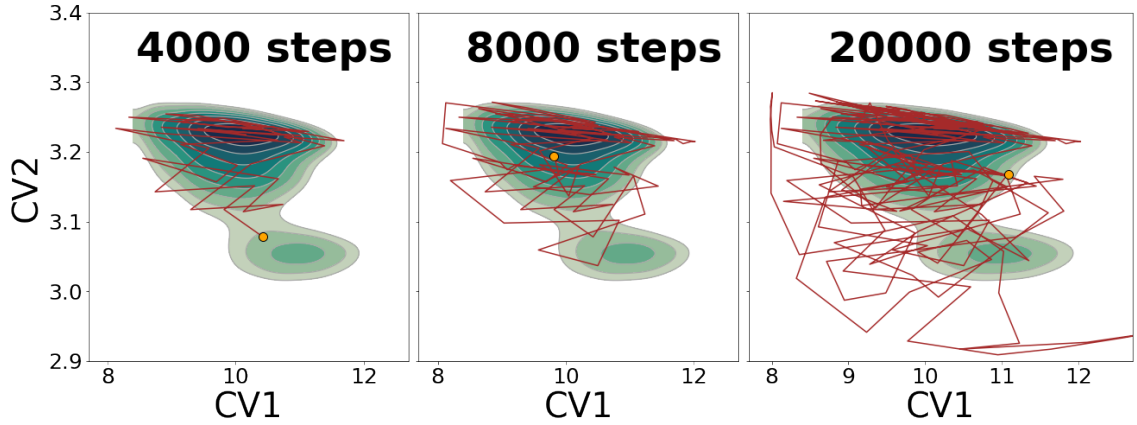

Figure D.9: First 4000, 8000 and 20000 steps of one Ag_6 WT-MTD trajectory (brown line) in CV1-CV2 space over the free energy surface at 10 K presented in Fig. 4.6. The points in the trajectory were taken each 100 steps. The Orange dot represents the position of the last step.

References

[1] Tsubasa Omoda, Shinjiro Takano, and Tatsuya Tsukuda. Toward Controlling the Electronic Structures of Chemically Modified Superatoms of Gold and Silver. *Small*, 17(27):2001439, jul 2021.

[2] Yun-Peng Xie, Yang-Lin Shen, Guang-Xiong Duan, Jun Han, Lai-Ping Zhang, and Xing Lu. Silver nanoclusters: synthesis, structures and photoluminescence. *Materials Chemistry Frontiers*, 4(8):2205–2222, 2020.

[3] M. Harb, F. Rabilloud, D. Simon, A. Rydlo, S. Lecoultre, F. Conus, V. Rodrigues, and C. Félix. Optical absorption of small silver clusters: Agn, (n=4-22). *Journal of Chemical Physics*, 129(19), 2008.

[4] Kaining Duanmu and Donald G. Truhlar. Validation of Methods for Computational Catalyst Design: Geometries, Structures, and Energies of Neutral and Charged Silver Clusters. *The Journal of Physical Chemistry C*, 119(17):9617–9626, apr 2015.

[5] Mingyang Chen, Jason E. Dyer, Keijing Li, and David A. Dixon. Prediction of Structures and Atomization Energies of Small Silver Clusters, (Ag) n , n < 100. *The Journal of Physical Chemistry A*, 117(34):8298–8313, aug 2013.

[6] A. V. Walker. Structure and energetics of small gold nanoclusters and their positive ions. *The Journal of Chemical Physics*, 122(9):094310, 2005.

[7] Bryan R. Goldsmith, Jacob Florian, Jin-Xun Liu, Philipp Gruene, Jonathan T. Lyon, David M. Rayner, André Fielicke, Matthias Scheffler, and Luca M. Ghiringhelli. Two-to-three dimensional transition in neutral gold clusters: The crucial role of van der Waals interactions and temperature. *Physical Review Materials*, 3(1):016002, jan 2019.

[8] Giovanni Bussi, Alessandro Laio, and Michele Parrinello. Equilibrium free energies from nonequilibrium processes. *Physical Review Letters*, 96(6):090601–1,4, 2006.

[9] Alessandro Barducci, Giovanni Bussi, and Michele Parrinello. Well-tempered metadynamics: A smoothly converging and tunable free-energy method. *Physical Review Letters*, 100(2):1–4, 2008.

[10] Vishal Agarwal, Paul J Dauenhauer, George W Huber, and Scott M Auerbach. Ab initio dynamics of cellulose pyrolysis: Nascent decomposition pathways at 327 and 600 c. *Journal of the American Chemical Society*, 134(36):14958–14972, 2012.

[11] Shaohui Zheng and Jim Pfaendtner. Enhanced sampling of chemical and biochemical reactions with metadynamics. *Molecular Simulation*, 41(1-3):55–72, feb 2015.

[12] Luis Petersen, Albert Ardèvol, Carme Rovira, and Peter J Reilly. Mechanism of cellulose hydrolysis by inverting gh8 endoglucanases: a qm/mm metadynamics study. *The Journal of Physical Chemistry B*, 113(20):7331–7339, 2009.

[13] Fabio Pietrucci and Wanda Andreoni. Graph theory meets ab initio molecular dynamics: Atomic structures and transformations at the nanoscale. *Phys. Rev. Lett.*, 107:085504, Aug 2011.

[14] Shu Liu, Rao Fu, Li Hua Zhou, and Sheng Ping Chen. Application of consensus scoring and principal component analysis for virtual screening against β-secretase (BACE-1). *PLoS ONE*, 7(6):e38086, 2012.

[15] Changru Ma, Simone Piccinin, and Stefano Fabris. Reaction Mechanisms of Water Splitting and H 2 Evolution by a Ru(II)-Pincer Complex Identified with Ab Initio Metadynamics Simulations. *ACS Catalysis*, 2(7):1500–1506, jul 2012.

[16] Jacopo Sgrignani, Giovanni Grazioso, Marco De Amici, and Giorgio Colombo. Inactivation of TEM-1 by Avibactam (NXL-104): Insights from Quantum Mechanics/Molecular Mechanics Metadynamics Simulations. *Biochemistry*, 53(31):5174–5185, aug 2014.

[17] Xevi Biarnés, Albert Ardevol, Antoni Planas, Carme Rovira, Alessandro Laio, and Michele Parrinello. The conformational free energy landscape of β-d-glucopyranose. implications for substrate preactivation in β-glucoside hydrolases. *Journal of the American Chemical Society*, 129(35):10686–10693, 2007.

[18] Mireille Ghoussoub, Shwetank Yadav, Kulbir Kaur Ghuman, Geoffrey A Ozin, and Chandra Veer Singh. Metadynamics-biased ab initio molecular dynamics study of heterogeneous co2 reduction via surface frustrated lewis pairs. *ACS Catalysis*, 6(10):7109–7117, 2016.

[19] Gianluca Santarossa, Angelo Vargas, Marcella Iannuzzi, and Alfons Baiker. Free energy surface of two- and three-dimensional transitions of Au 12 nanoclusters obtained by ab initio metadynamics. *Physical Review B*, 81(17):174205, may 2010.

[20] Benjamin Evangelisti, Kristen A. Fichthorn, and Adri C.T. Van Duin. Development and initial applications of an e-ReaxFF description of Ag nanoclusters. *Journal of Chemical Physics*, 153(10), 2020.

[21] WD Knight, Keith Clemenger, Walt A de Heer, Winston A Saunders, MY Chou, and Marvin L Cohen. Electronic shell structure and abundances of sodium clusters. *Physical review letters*, 52(24):2141, 1984.

[22] Robert G Parr and Weitao Yang. *Density-Functional Theory of Atoms and Molecules, vol. 16 of International series of monographs on chemistry*. Oxford University Press, New York, 1989.

[23] Frank Jensen. *Introduction to computational chemistry*. John wiley & sons, 2017.

[24] Pierre Hohenberg and Walter Kohn. Inhomogeneous electron gas. *Physical review*, 136(3B):B864, 1964.

[25] Walter Kohn and Lu Jeu Sham. Self-consistent equations including exchange and correlation effects. *Physical review*, 140(4A):A1133, 1965.

[26] John P Perdew, Kieron Burke, and Matthias Ernzerhof. Generalized gradient approximation made simple. *Physical review letters*, 77(18):3865, 1996.

[27] Sérgio Filipe Sousa, Pedro Alexandrino Fernandes, and Maria Joao Ramos. General performance of density functionals. *The Journal of Physical Chemistry A*, 111(42):10439–10452, 2007.

[28] Claude Cohen-Tannoudji, Bernard Diu, Frank Laloe, and Bernard Dui. Quantum mechanics (2 vol. set), 2006.

[29] A. Warshel and M. Levitt. Theoretical studies of enzymic reactions: Dielectric, electrostatic and steric stabilization of the carbonium ion in the reaction of lysozyme. *Journal of Molecular Biology*, 103(2):227–249, 1976.

[30] Asmus O. Dohn. Multiscale electrostatic embedding simulations for modeling structure and dynamics of molecules in solution: A tutorial review. *International Journal of Quantum Chemistry*, 120(21):1–22, 2020.

[31] Hiroshi C. Watanabe and Qiang Cui. Quantitative Analysis of QM/MM Boundary Artifacts and Correction in Adaptive QM/MM Simulations. *Journal of Chemical Theory and Computation*, 15(7):3917–3928, 2019.

[32] Maria Karelina and Heather J. Kulik. Systematic Quantum Mechanical Region Determination in QM/MM Simulation. *Journal of Chemical Theory and Computation*, 13(2):563–576, 2017.

[33] Alessandro Laio, Joost VandeVondele, and Ursula Rothlisberger. A hamiltonian electrostatic coupling scheme for hybrid car–parrinello molecular dynamics simulations. *The Journal of chemical physics*, 116(16):6941–6947, 2002.

[34] Joshua A Rackers and Jay W Ponder. Classical pauli repulsion: An anisotropic, atomic multipole model. *The Journal of chemical physics*, 150(8):084104, 2019.

[35] Alireza Marefat Khah, Peter Reinholdt, Jógvan Magnus Haugaard Olsen, Jacob Kongsted, and Christof Hattig. Avoiding electron spill-out in qm/mm calculations on excited states with simple pseudopotentials. *Journal of Chemical Theory and Computation*, 16(3):1373–1381, 2020.

[36] Hai Lin and Donald G. Truhlar. QM/MM: What have we learned, where are we, and where do we go from here? *Theoretical Chemistry Accounts*, 117(2):185–199, 2007.

[37] Elizabeth Brunk and Ursula Rothlisberger. Mixed Quantum Mechanical/Molecular Mechanical Molecular Dynamics Simulations of Biological Systems in Ground and Electronically Excited States. *Chemical reviews*, 115(12):6217–6263, apr 2015.

[38] Walter Greiner, Ludwig Neise, and Horst Stöcker. *Thermodynamics and statistical mechanics*. Springer Science & Business Media, 2012.

[39] Michael Brin and Garrett Stuck. *Introduction to dynamical systems*. Cambridge university press, 2002.

[40] Daniel M Zuckerman. *Statistical physics of biomolecules: an introduction*. CRC Press, 2010.

[41] Frederick Reif. *Fundamentals of statistical and thermal physics*. Waveland Press, 2009.

[42] William Coffey and Yu P Kalmykov. *The Langevin equation: with applications to stochastic problems in physics, chemistry and electrical engineering*, volume 27. World Scientific, 2012.

[43] H. J.C. Berendsen, J. P.M. Postma, W. F. Van Gunsteren, A. Dinola, and J. R. Haak. Molecular dynamics with coupling to an external bath. *The Journal of Chemical Physics*, 81(8):3684–3690, 1984.

[44] Paul Bauer, Berk Hess, and Erik Lindahl. Gromacs 2022.1 manual, April 2022.

[45] Agnes Lagnoux. Rare event simulation. *Probability in the Engineering and Informational Sciences*, 20(1):45–66, 2006.

[46] Glenn M Torrie and John P Valleau. Nonphysical sampling distributions in monte carlo free-energy estimation: Umbrella sampling. *Journal of Computational Physics*, 23(2):187–199, 1977.

[47] Pu Liu, Byungchan Kim, Richard A Friesner, and BJ Berne. Replica exchange with solute tempering: A method for sampling biological systems in explicit water. *Proceedings of the National Academy of Sciences*, 102(39):13749–13754, 2005.

[48] Rafael C Bernardi, Marcelo CR Melo, and Klaus Schulten. Enhanced sampling techniques in molecular dynamics simulations of biological systems. *Biochimica et Biophysica Acta (BBA)-General Subjects*, 1850(5):872–877, 2015.

[49] Christophe Chipot and Andrew Pohorille. Free energy calculations. *Springer series in chemical physics*, 86:159–184, 2007.

[50] Alessandro Barducci, Massimiliano Bonomi, and Michele Parrinello. Metadynamics. *Wiley Interdisciplinary Reviews: Computational Molecular Science*, 1(5):826–843, 2011.

[51] Thomas Ludwig, Aayush R Singh, and Jens K Nørskov. Subsurface nitrogen dissociation kinetics in lithium metal from metadynamics. *The Journal of Physical Chemistry C*, 124(48):26368–26378, 2020.

[52] Alessandro Barducci, Giovanni Bussi, and Michele Parrinello. Well-tempered metadynamics: a smoothly converging and tunable free-energy method. *Physical review letters*, 100(2):020603, 2008.

[53] Ask Hjorth Larsen, Jens Jørgen Mortensen, Jakob Blomqvist, Ivano E Castelli, Rune Christensen, Marcin Dułak, Jesper Friis, Michael N Groves, Bjørk Hammer, Cory Hargus, Eric D Hermes, Paul C Jennings, Peter Bjerre Jensen, James Kermode, John R Kitchin, Esben Leonhard Kolsbjerg, Joseph Kubal, Kristen Kaasbjerg, Steen Lysgaard, Jón Bergmann Maronsson, Tristan Maxson, Thomas Olsen, Lars Pastewka,

Andrew Peterson, Carsten Rostgaard, Jakob Schiøtz, Ole Schütt, Mikkel Strange, Kristian S Thygesen, Tejs Vegge, Lasse Vilhelmsen, Michael Walter, Zhenhua Zeng, and Karsten W Jacobsen. The atomic simulation environment—a python library for working with atoms. *Journal of Physics: Condensed Matter*, 29(27):273002, 2017.

[54] M. J. Frisch, G. W. Trucks, H. B. Schlegel, G. E. Scuseria, M. A. Robb, J. R. Cheeseman, G. Scalmani, V. Barone, G. A. Petersson, H. Nakatsuji, X. Li, M. Caricato, A. V. Marenich, J. Bloino, B. G. Janesko, R. Gomperts, B. Mennucci, H. P. Hratchian, J. V. Ortiz, A. F. Izmaylov, J. L. Sonnenberg, D. Williams-Young, F. Ding, F. Lipparini, F. Egidi, J. Goings, B. Peng, A. Petrone, T. Henderson, D. Ranasinghe, V. G. Zakrzewski, J. Gao, N. Rega, G. Zheng, W. Liang, M. Hada, M. Ehara, K. Toyota, R. Fukuda, J. Hasegawa, M. Ishida, T. Nakajima, Y. Honda, O. Kitao, H. Nakai, T. Vreven, K. Throssell, J. A. Montgomery, Jr., J. E. Peralta, F. Ogliaro, M. J. Bearpark, J. J. Heyd, E. N. Brothers, K. N. Kudin, V. N. Staroverov, T. A. Keith, R. Kobayashi, J. Normand, K. Raghavachari, A. P. Rendell, J. C. Burant, S. S. Iyengar, J. Tomasi, M. Cossi, J. M. Millam, M. Klene, C. Adamo, R. Cammi, J. W. Ochterski, R. L. Martin, K. Morokuma, O. Farkas, J. B. Foresman, and D. J. Fox. Gaussian 16 Revision C.01, 2016. Gaussian Inc. Wallingford CT.

[55] Thomas D Kühne, Marcella Iannuzzi, Mauro Del Ben, Vladimir V Rybkin, Patrick Seewald, Frederick Stein, Teodoro Laino, Rustam Z Khaliullin, Ole Schütt, Florian Schiffmann, et al. Cp2k: An electronic structure and molecular dynamics software package-quickstep: Efficient and accurate electronic structure calculations. *The Journal of Chemical Physics*, 152(19):194103, 2020.

[56] Mark James Abraham, Teemu Murtola, Roland Schulz, Szilárd Páll, Jeremy C. Smith, Berk Hess, and Erik Lindah. Gromacs: High performance molecular simulations through multi-level parallelism from laptops to supercomputers. *SoftwareX*, 1-2:19–25, 2015.

[57] Aidan P Thompson, H Metin Aktulga, Richard Berger, Dan S Bolintineanu, W Michael Brown, Paul S Crozier, Pieter J in't Veld, Axel Kohlmeyer, Stan G Moore, Trung Dac Nguyen, et al. Lammps-a flexible simulation tool for particle-based materials modeling at the atomic, meso, and continuum scales. *Computer Physics Communications*, page 108171, 2021.

[58] Jens Jørgen Mortensen, Lars Bruno Hansen, and Karsten Wedel Jacobsen. Real-space grid implementation of the projector augmented wave method. *Physical Review B*, 71(3):035109, 2005.

[59] Peter E Blöchl. Projector augmented-wave method. *Physical review B*, 50(24):17953, 1994.

[60] Jussi Enkovaara, Carsten Rostgaard, J Jørgen Mortensen, Jingzhe Chen, M Dułak, Lara Ferrighi, Jeppe Gavnholt, Christian Glinsvad, V Haikola, HA Hansen, et al. Electronic structure calculations with gpaw: a real-space implementation of the projector augmented-wave method. *Journal of physics: Condensed matter*, 22(25):253202, 2010.

[61] Ask Hjorth Larsen, Marco Vanin, Jens Jørgen Mortensen, Kristian Sommer Thygesen, and Karsten Wedel Jacobsen. Localized atomic basis set in the projector augmented wave method. *Physical Review B*, 80(19):195112, 2009.

[62] Gareth A. Tribello, Massimiliano Bonomi, Davide Branduardi, Carlo Camilloni, and Giovanni Bussi. PLUMED 2: New feathers for an old bird. *Computer Physics Communications*, 185(2):604–613, 2014.

[63] T. L. Haslett, K. A. Bosnick, and M. Moskovits. Ag5 is a planar trapezoidal molecule. *Journal of Chemical Physics*, 108(9):3453–3457, 1998.

[64] V. Bonačić-Koutecký, L. Češpiva, P. Fantucci, and J. Koutecký. Effective core potential-configuration interaction study of electronic structure and geometry of small neutral and cationic Ag n clusters: Predictions and interpretation of measured properties. *The Journal of Chemical Physics*, 98(10):7981–7994, may 1993.

[65] Lara Ferrighi, Bjork Hammer, and Georg K. H. Madsen. 2d-3d transition for cationic and anionic gold clusters: A kinetic energy density functional study. *Journal of the American Chemical Society*, 131(30):10605–10609, 2009.

[66] S. Lecoultre, A. Rydlo, J. Buttet, C. Félix, S. Gilb, and W. Harbich. Ultraviolet-visible absorption of small silver clusters in neon: Ag n (n = 1–9). *The Journal of Chemical Physics*, 134(18):184504, may 2011.

[67] Andrew W Long and Andrew L Ferguson. Rational design of patchy colloids via landscape engineering. *Molecular Systems Design & Engineering*, 3(1):49–65, 2018.

[68] Mohammad M Sultan and Vijay S Pande. Automated design of collective variables using supervised machine learning. *The Journal of chemical physics*, 149(9):094106, 2018.

[69] Dan Mendels, Giovannimaria Piccini, Z Faidon Brotzakis, Yi I Yang, and Michele Parrinello. Folding a small protein using harmonic linear discriminant analysis. *The Journal of chemical physics*, 149(19):194113, 2018.

[70] Paolo Raiteri, Alessandro Laio, Francesco Luigi Gervasio, Cristian Micheletti, and Michele Parrinello. Efficient reconstruction of complex free energy landscapes by multiple walkers metadynamics. *The journal of physical chemistry B*, 110(8):3533–3539, 2006.

[71] Hadi Mehrabian and Bernhardt L Trout. In silico engineering of hydrate anti-agglomerant molecules using bias-exchange metadynamics simulations. *The Journal of Physical Chemistry C*, 124(35):18983–18992, 2020.

[72] Christopher D Fu, Luiz FL Oliveira, and Jim Pfaendtner. Assessing generic collective variables for determining reaction rates in metadynamics simulations. *Journal of Chemical Theory and Computation*, 13(3):968–973, 2017.

[73] Giovanni Bussi, Davide Branduardi, et al. Free-energy calculations with metadynamics: Theory and practice. *Rev. Comput. Chem*, 28:1–49, 2015.

[74] Fabien Conus, J Tobias Lau, Varlei Rodrigues, and Christian Félix. High sensitivity absorption measurement of small metal clusters embedded in an argon matrix. *Review of scientific instruments*, 77(11):113103, 2006.

[75] Eyal Neria, Stefan Fischer, and Martin Karplus. Simulation of activation free energies in molecular systems. *The Journal of chemical physics*, 105(5):1902–1921, 1996.

[76] Giovanni Ciccotti, Mauro Ferrario, and J-P Ryckaert. Molecular dynamics of rigid systems in cartesian coordinates a general formulation. *Molecular Physics*, 47(6):1253–1264, 1982.

[77] Ivan Sondi and Branka Salopek-Sondi. Silver nanoparticles as antimicrobial agent: a case study on e. coli as a model for gram-negative bacteria. *Journal of colloid and interface science*, 275(1):177–182, 2004.

[78] Kaiyuan Zheng, Magdiel I Setyawati, Tze-Peng Lim, David Tai Leong, and Jianping Xie. Antimicrobial cluster bombs: silver nanoclusters packed with daptomycin. *ACS nano*, 10(8):7934–7942, 2016.